

# A critical review of the absorption cross-sections of O<sub>3</sub> and NO<sub>2</sub> in the ultraviolet and visible<sup>☆</sup>

J. Orphal\*

Laboratoire de Photophysique Moléculaire, CNRS, Bât. 350, Centre d'Orsay, Orsay 91405 Cedex, France

Received 10 July 2002; received in revised form 19 September 2002; accepted 19 September 2002

## Abstract

The available laboratory measurements of UV-Vis (240–790 nm) absorption cross-sections of O<sub>3</sub> and NO<sub>2</sub> are critically reviewed taking into account the variation of the cross-sections with temperature (in the 200–300 K range) and with total pressure (<1 atm).

© 2003 Elsevier Science B.V. All rights reserved.

**Keywords:** Absorption; Cross-section; Review; Ozone; O<sub>3</sub>; NO<sub>2</sub>

## 1. Introduction

The changing atmosphere of the Earth is a subject of great public and political interest [1–6]. Three topics are currently of major concern: (1) the destruction of the stratospheric ozone layer that protects life from harmful solar ultraviolet (UV) radiation, (2) the pollution of the troposphere by trace gases that lead to changes in the oxidising capacity of the atmosphere and are harmful for human health, and (3) the significant increase of the so-called “greenhouse” gases that absorb little in the UV-Vis where solar radiation has its maximum but strongly in the infrared region where the Earth's emission is strongest, thereby decreasing the cooling cycle of the Earth system. In this context, the long-term monitoring of the Earth's atmosphere on a global scale is essential to identify and to understand changes, and to predict the evolution by chemical and climate models. However, ground- or air-borne instruments can only cover parts of the atmosphere. Therefore, atmospheric remote-sensing by satellite instruments is the only tool to provide the necessary data.

In the past decade, a new generation of multi-spectral remote-sensing instruments using medium-resolution diode-array spectrometers in the ultraviolet, visible, and near-infrared has been developed. Since the successful launch of the first of these new experiments, GOME [7] onboard ERS-2 in 1995, it is possible to study global O<sub>3</sub>

concentrations using the full spectral information in the 240–790 nm region. Besides the improved accuracy for the O<sub>3</sub> measurements that results from this broad spectral coverage at medium resolution (including O<sub>3</sub> profile retrieval), it is possible to detect many other species of atmospheric relevance (NO<sub>2</sub>, H<sub>2</sub>O, BrO, OCIO, SO<sub>2</sub>, H<sub>2</sub>CO, NO<sub>3</sub>) as well as atmospheric properties such as cloud coverage, cloud optical depth, aerosols distributions, surface albedo, etc.

GOME was followed by the SCIAMACHY [8,9] instrument (launched in march 2002 onboard ENVISAT-1), and will be continued by the GOME-2 instruments onboard the METOP satellites (first launch in 2004), by the OMI instruments onboard EOS-Aura (launch in 2004) and by other UV-Vis spectrometers using diode-array detectors (e.g. MAESTRO onboard ACE, to be launched in 2003). In order to derive trace gas concentrations from the atmospheric spectra, accurate reference spectra for each absorber at the relevant atmospheric conditions (temperature and pressure) are indispensable [10]. However, today there are many different laboratory measurements available, with different experimental conditions (spectral resolution, spectral regions covered, sample temperature and total pressure, etc.) and with varying accuracies. It is, therefore, important to compare this data and to identify discrepancies and systematic errors.

In this paper, we report a review of the available laboratory measurements of the absorption cross-sections of O<sub>3</sub> and NO<sub>2</sub> for the new atmospheric remote-sensing instruments. It is a difficult task to compare laboratory measurements. We have, therefore, used several methods to take into account possible sources for systematic errors: studying the influence of resolution and wavelength accuracy on the

<sup>☆</sup> This paper is a modified and significantly reduced version of the ESA Technical Note MO-TN-ESA-GO-0302, published by the European Space Agency, ESTEC, Noordwijk, 2002, in two volumes.

\* Tel.: +33-1-6915-752886; fax: +1-6915-753055.

E-mail address: [Johannes.orphal@ppm.u-psud.fr](mailto:Johannes.orphal@ppm.u-psud.fr) (J. Orphal).

cross-sections, comparing the cross-sections at single wavelengths, comparing the cross-sections over broad spectral regions, comparing integrated cross-sections, studying the influence of temperature, using non-linear least-squares fits in regions where the cross-sections vary rapidly with wavelength, and comparing different approaches to model the temperature dependence of the absorption cross-sections.

## 2. Ozone

### 2.1. The $O_3$ absorption spectrum in the 240–790 nm region

The  $O_3$  absorption cross-sections in the 240–790 nm region can be separated into four systems: the Hartley band, the Huggins bands, the Chappuis band, and the Wulf bands extending towards longer wavelengths (see Fig. 1).

The Hartley band is the strongest band extending from about 200–320 nm and peaks around 255 nm. Although its overall shape is very smooth, determined by the short lifetime of  $O_3$  in the upper electronic state due to rapid photodissociation, there is a residual vibrational structure (see Fig. 2), due to quasiperiodical orbits of the electronic wavepackets before dissociation in the upper state, a structure that is slightly temperature-dependent (due to the change of the Franck–Condon point with temperature). Although the overall structure of the Hartley band is theoretically well understood, there is currently no calculation that is able to predict the absorption cross-sections of  $O_3$  within experimental accuracy or better.

The Huggins bands consists of a series of individual peaks extending from about 300–390 nm (see Fig. 3), showing a

strong temperature dependence due to the varying slope of the Hartley band and to the sharpening of the individual bands at lower temperatures. Due to the drastic change of the cross-sections with wavelength (over more than five-orders of magnitude) it is impossible to measure the entire Huggins band system at once (i.e. with the same combination of absorption path and  $O_3$  partial pressure). In the past, several analytical expressions have been proposed to interpolate the temperature-dependence of the absorption cross-sections in this region. The Huggins bands are currently used for spectroscopic remote-sensing of  $O_3$  by many experimental techniques (Dobson spectrometers, Brewer spectrometers, TOMS, DOAS, etc.).

The Chappuis band is a broad structure in the visible region between about 380 and 800 nm which is more than thousand times weaker than the Hartley band (see Fig. 4). The residual structures (similar to those observed in the Hartley band) arise from quantum mechanical interferences between two interacting excited electronic states and show only little variation with temperature. The region between 400 and 500 nm is also used for atmospheric remote-sensing of  $O_3$  from ground, air- and space-borne sensors.

For all these bands in the 240–790 nm region, there exists a large number of laboratory measurements using different spectrometers and experimental conditions [11–61]. Note that many new measurements have been published in the past 15 years [36–61].

In the following sections, several approaches will be used for comparing the  $O_3$  absorption cross-sections: absolute values at selected wavelengths, absolute values over large regions, integrated cross-sections, and non-linear least-squares fits.

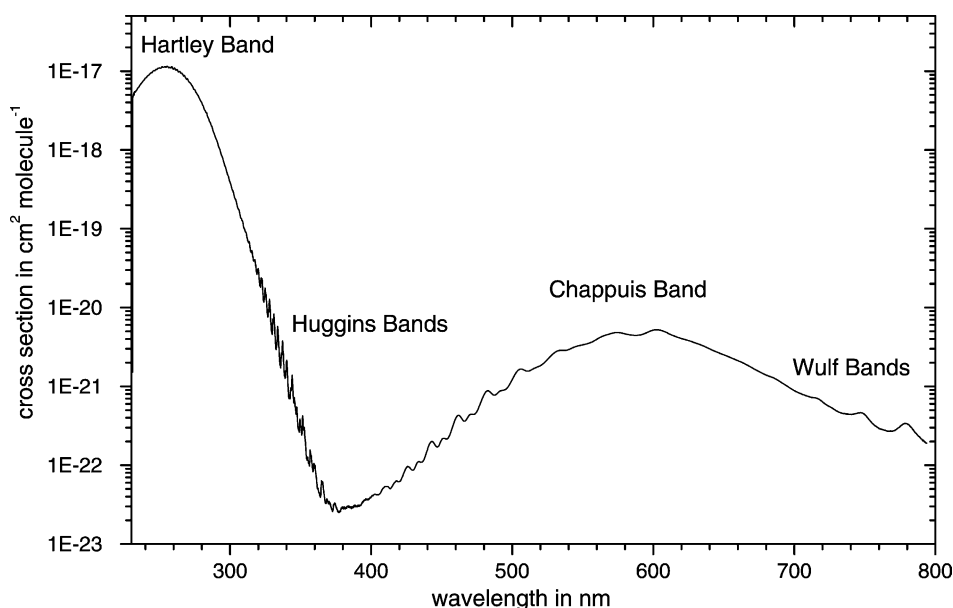


Fig. 1. The  $O_3$  spectrum at room temperature (source: Richter et al.).

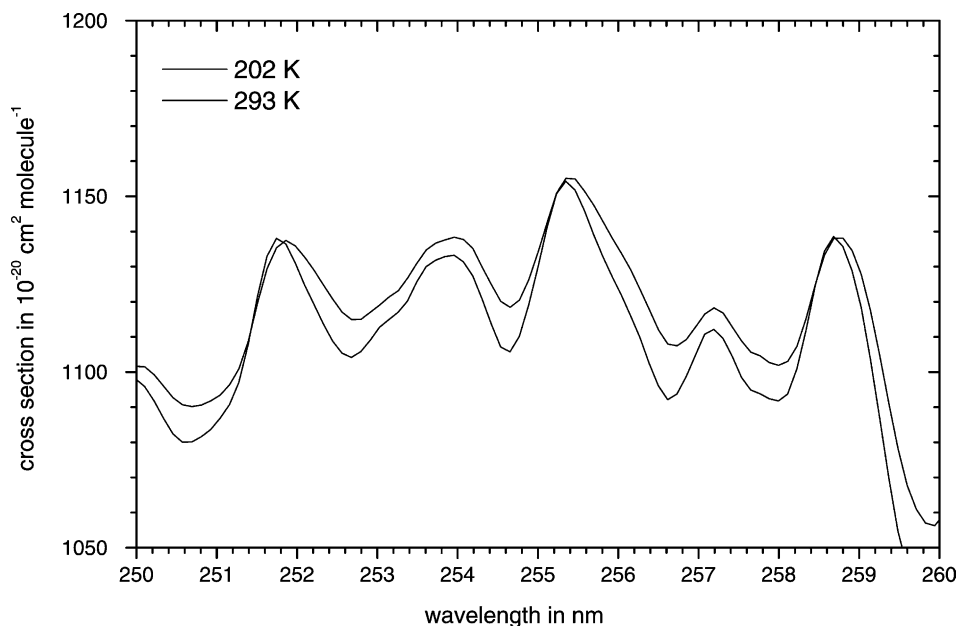


Fig. 2. The  $O_3$  cross-sections at the peak of the Hartley band (source: Richter et al.).

## 2.2. Relative change of the $O_3$ spectrum with spectral resolution and wavelength shifts

In a first step, we have investigated the sensitivity of the  $O_3$  spectrum to wavelength calibration and to spectral resolution, in order to assess their influence on the absorption cross-sections which will be compared afterwards. It is important to stress the fact that, since relative changes are studied, the differing absolute values of the cross-sections and the wavelength calibration errors in the experimental

data are not showing up in these comparisons. Two examples are given in Figs. 5 and 6. The results have been validated using different sets of laboratory data and are grouped in three regions: 240–310, 310–410, and 410–790 nm. The region between 310 and 410 nm requires special attention due to the strong differential structures present here.

In the 240–790 nm region (except between 310 and 410 nm), the  $O_3$  spectrum changes by <1% for wavelength shifts of 0.05 nm or less. In the 240–790 nm region (except

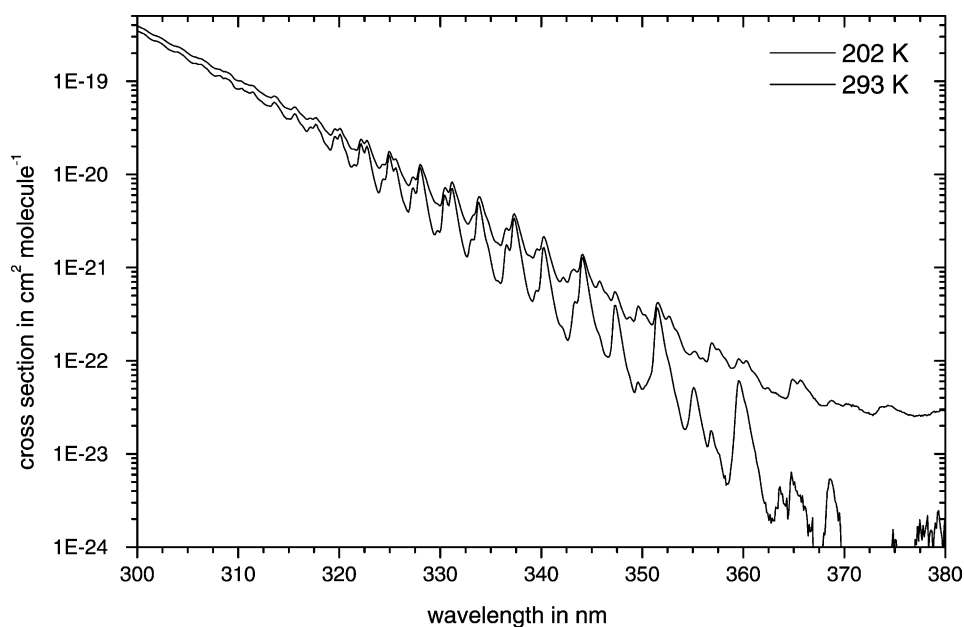


Fig. 3. The  $O_3$  cross-sections in the Huggins bands (source: Richter et al.).

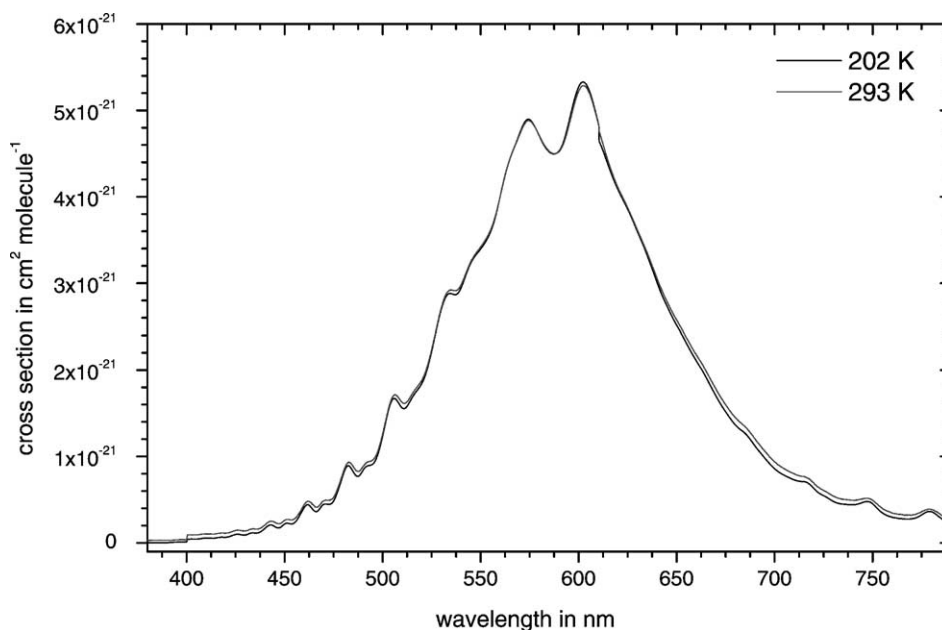


Fig. 4. The O<sub>3</sub> cross-sections in the Chappuis band (source: Richter et al.).

between 310 and 410 nm), the O<sub>3</sub> spectrum changes by <0.2% when the spectrum is convoluted with a Gaussian of 0.1 nm FWHM, and by <0.05% when the spectrum is convoluted with a Gaussian of 0.01 nm FWHM. In the 310–410 nm region, the O<sub>3</sub> spectrum (at spectral resolutions of 0.025 nm or better) changes by up to 20% for wavelength shifts of 0.05 nm and by up to 7% for wavelength shifts of 0.01 nm. In this region (310–410 nm) the changes in the O<sub>3</sub> spectrum

for different wavelength shifts are resolution-dependent: for lower resolution (e.g. for the GOME-FM spectra at a spectral resolution of about 0.2 nm) wavelength shifts of 0.05 nm introduce changes in the O<sub>3</sub> spectrum of up to 9% and even shifts of only 0.01 nm still introduce changes of up to 1.5%. In the 310–410 nm region, the O<sub>3</sub> spectrum changes by up to 9% after convolution with a Gaussian of 0.1 nm FWHM by up to 0.2% after convolution with a Gaussian of 0.01 nm.

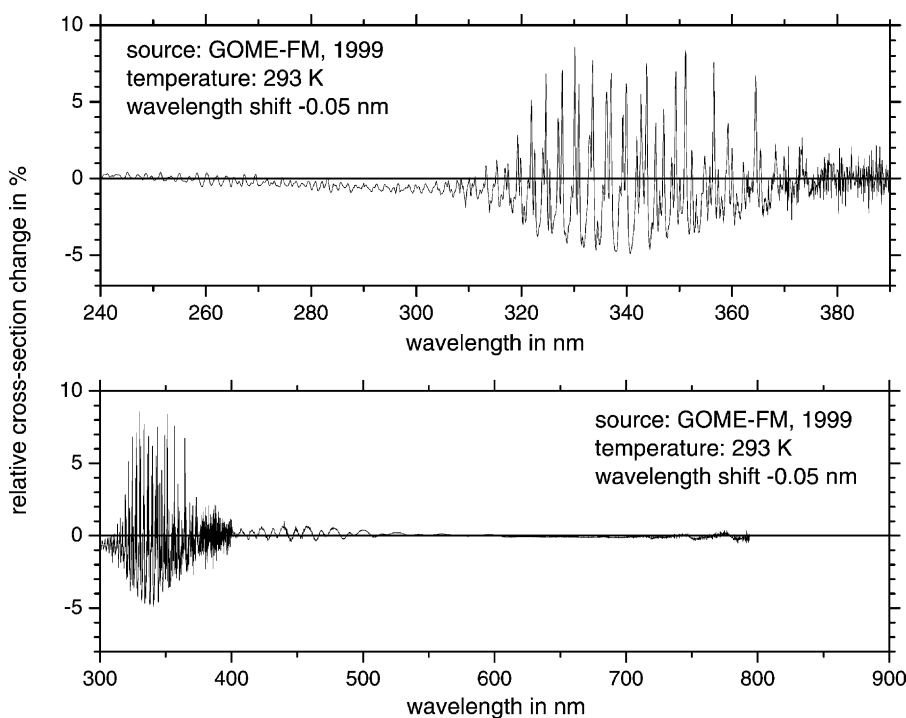


Fig. 5. Relative change of the O<sub>3</sub> spectrum (source: [7,8,55,90] spectral resolution ca. 0.2–0.4 nm) after a wavelength shift of  $-0.01$  nm.

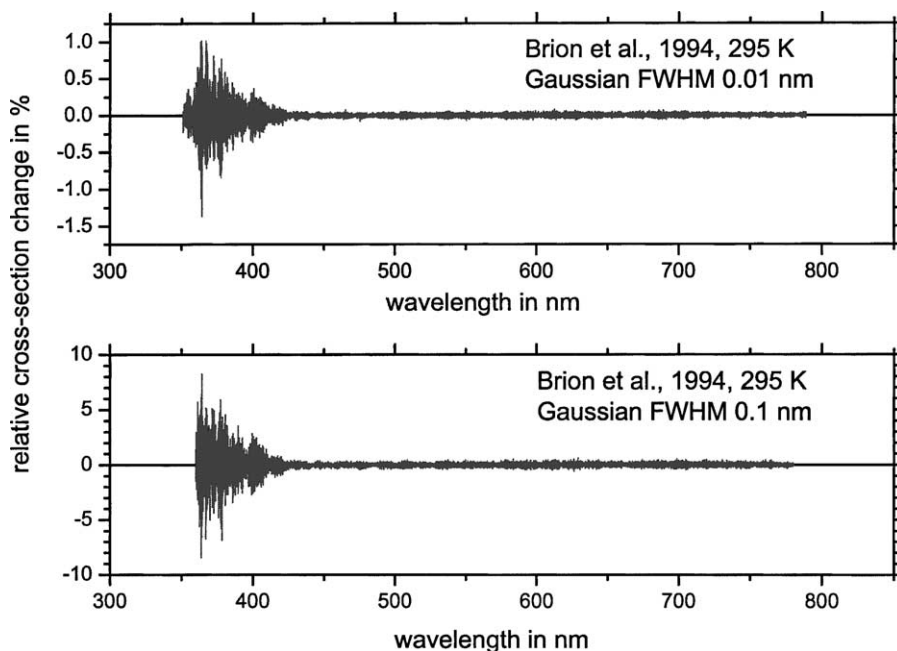


Fig. 6. Relative change of the  $O_3$  spectrum (source: [30,31,48,53] spectral resolution ca. 0.01 nm) after convolution with a Gaussian function of 0.01 nm FWHM and of 0.1 nm FWHM.

Unfortunately there are only few laboratory measurements at very high resolution (0.01 nm or better) and with very accurate wavelength calibration (0.01 nm or better).

### 2.3. Relative change of the $O_3$ spectrum with total pressure

A second important point was to study the relative change of the  $O_3$  spectrum with total pressure, as a potential source for systematic differences between different laboratory measurements. However, at present, there is no experimental or theoretical support for a pressure dependence of the  $O_3$  cross-sections in the entire spectral region 240–790 nm, although one group [60] has proposed that temperature-dependent variations of the cross-sections in the region around 400 nm might be due to the formation of

a weakly-bounded  $O_2$ – $O_3$  complex. Note that the  $O_3$  dimer has been predicted by theory and was observed recently in low-temperature matrices [62,63]. However, for the remainder of this paper, we will not consider differences in total pressure in the various laboratory experiments, because the effects of  $O_2$ – $O_3$  complex formation—if they exist at all—on the  $O_3$  cross-sections are very small.

### 2.4. Comparison of the $O_3$ cross-sections between 230 and 790 nm at $298 \pm 5$ K

#### 2.4.1. $O_3$ cross-sections at single wavelengths

Using data from different experiments, average  $O_3$  cross-sections at room temperature ( $298 \pm 3$  K) were calculated at 10 single wavelengths between 253.65 and 632.82 nm, with uncertainties between 0.7 and 2.0%. The

Table 1  
Average absorption cross-sections of  $O_3^a$  at  $298 \pm 5$  K

Wavelength (nm)	Value ( $\times 10^{-20}$ cm $^2$ )	Uncertainty ( $\times 10^{-20}$ cm $^2$ )	Uncertainty (%)	Number of experimental data	Dispersion of experimental data
253.65	1141	10	0.9	17	[−1.3%, +1.4%]
289.36	149	3	2.0	13	[−3.4%, +3.4%]
296.73	60.3	0.9	1.6	13	[−5.2%, +4.2%]
302.15	29.2	0.5	1.8	12	[−2.7%, +4.1%]
543.52	0.0314	$4 \times 10^{-4}$	1.4	8	[−1.4%, +1.9%]
576.96	0.0477	$4 \times 10^{-4}$	0.8	10	[−6.1%, +1.9%]
594.10	0.0470	$6 \times 10^{-4}$	1.2	8	[−1.9%, +2.1%]
604.61	0.0522	$5 \times 10^{-4}$	0.9	7	[−2.5%, +0.9%]
611.97	0.0466	$4 \times 10^{-4}$	0.7	7	[−2.5%, +0.9%]
632.82	0.0346	$4 \times 10^{-4}$	1.2	7	[−1.2%, +2.3%]

<sup>a</sup> The cross-sections are given in units of  $10^{-20}$  cm $^2$ . Uncertainties are  $1\sigma$ .

Table 2  
Integrated absorption cross-sections of O<sub>3</sub><sup>a</sup> at 298 ± 5 K

Reference	Hartley band	Chappuis band	Huggins band	Blue tail of the Chappuis band
Bass and Paur [27,33,34]	3.55 × 10 <sup>-16</sup> (±0.0%)	–	8.20 × 10 <sup>-20</sup> (–1.2%)	–
Brion et al. [30,31,43,47,48,52]	3.52 × 10 <sup>-16</sup> (–0.8%)	–	8.32 × 10 <sup>-20</sup> (+0.3%)	–
Richter et al. <sup>b</sup>	3.53 × 10 <sup>-16</sup> (–0.6%)	6.47 × 10 <sup>-19</sup> (+1.6%)	8.25 × 10 <sup>-20</sup> (–0.6%)	7.23 × 10 <sup>-20</sup> (+8.4%)
Burrows et al. [55]	3.57 × 10 <sup>-16</sup> (+0.6%)	6.45 × 10 <sup>-19</sup> (+1.2%)	8.35 × 10 <sup>-20</sup> (+0.6%)	6.75 × 10 <sup>-20</sup> (+1.1%)
Voigt et al. [54,56,60]	3.58 × 10 <sup>-16</sup> (+0.8%)	6.42 × 10 <sup>-19</sup> (+0.7%)	8.35 × 10 <sup>-20</sup> (+0.6%)	6.75 × 10 <sup>-20</sup> (+1.1%)
Bogumil et al. [57–59,61]	3.55 × 10 <sup>-16</sup> (±0.0%)	6.41 × 10 <sup>-19</sup> (+0.5%)	8.33 × 10 <sup>-20</sup> (+0.4%)	6.52 × 10 <sup>-20</sup> (–2.2%)
Burkholder and Talukdar [51]	–	6.21 × 10 <sup>-19</sup> (–2.6%)	–	6.35 × 10 <sup>-20</sup> (–4.8%)
Brion et al. [53]	–	6.29 × 10 <sup>-19</sup> (–1.3%)	–	6.43 × 10 <sup>-20</sup> (–3.6%)
Average value relative uncertainty	3.55 × 10 <sup>-16</sup> (±0.6%)	6.38 × 10 <sup>-19</sup> (±1.6%)	8.30 × 10 <sup>-20</sup> (±0.7%)	6.67 × 10 <sup>-20</sup> (±4.8%)

<sup>a</sup> The integrated cross-sections are given in units of cm<sup>2</sup> × nm.

<sup>b</sup> Unpublished values based on the data of [55].

results are summarized in Table 1. The average values given in this table are those determined after eliminating measurements having larger deviations than the stated experimental uncertainties. Clearly, there is a large gap between 302 and 543 nm, which cannot be filled by simple comparisons of the experimental data.

#### 2.4.2. Integrated O<sub>3</sub> cross-sections

Because the integrated absorption cross-sections are rather insensitive to differences in spectral resolution and wavelength calibration, we have calculated these values for the following regions:

- in the Hartley band between 245 and 340 nm;
- in the Chappuis band between 410 and 690 nm;
- in the Huggins bands between 325 and 340 nm;
- in the blue tail of the Chappuis band between 410 and 520 nm.

The results are shown in Table 2. One can state that the agreement between the different data is better than 1.2% for the Hartley and Huggins bands, but less (up to 2.7%) for the Chappuis band, and much less for the blue tail of the Chappuis band.

#### 2.4.3. Comparison of the O<sub>3</sub> cross-sections in the Huggins bands

To compare the available O<sub>3</sub> absorption cross-sections in the Huggins bands, a different approach is required. Because

of the strong influence of small wavelength shifts and of the spectral resolution, we have used the following procedure, in the region 323–343 nm:

- all spectra were convoluted with a Gaussian with a 0.4 nm FWHM;
- the spectra were compared using a non-linear least-squares fitting program, with five fitting parameters: a quadratic polynomial (three parameters) accounting for small baseline differences, a scaling coefficient accounting for differences in the absolute magnitude of the cross-sections (one parameter), and a linear wavelength shift coefficient (one parameter) accounting for differences in the wavelength calibration.

The convolution is employed to minimize the influence of spectral resolution when comparing cross-sections recorded at high spectral resolution with cross-sections recorded at lower resolution. The non-linear least-squares fitting program is employed to minimize the influence of wavelength shifts and of baseline drifts or straylight. We have verified that the convolution does not change the scaling and shifting parameters within the experimental uncertainties.

Two examples of the fits are given in Figs. 7 and 8. Using the relative differences obtained from the non-linear least-squares fits, we have determined the relative differences of each individual spectrum to the average values (taking into account the different wavelength shifts and the baseline differences) for the O<sub>3</sub> cross-sections in this

Table 3  
Comparison of O<sub>3</sub> cross-sections in the Huggins bands at 298 ± 5 K using a non-linear least-squares fit approach

Reference 1	Reference 2	Shift (nm)	Scaling factor	Scale to mean
–	Bass and Paur [27,33,34]	–	1.000	0.996
Bass and Paur [27,33,34]	Brion et al. [47,48,52]	–0.043	1.001	0.997
Bass and Paur [27,33,34]	Voigt et al. [54,56,60]	–0.029	0.956	0.953
Bass and Paur [27,33,34]	Richter et al. <sup>a</sup>	–0.013	1.014	1.010
Bass and Paur [27,33,34]	Burrows et al. [55]	–0.013	1.002	0.965
Bass and Paur [27,33,34]	Bogumil et al. [57–59,61]	–0.015	1.049	1.045

Mean: 1.004 ± 0.030.

<sup>a</sup> Unpublished values based on the data of [55].

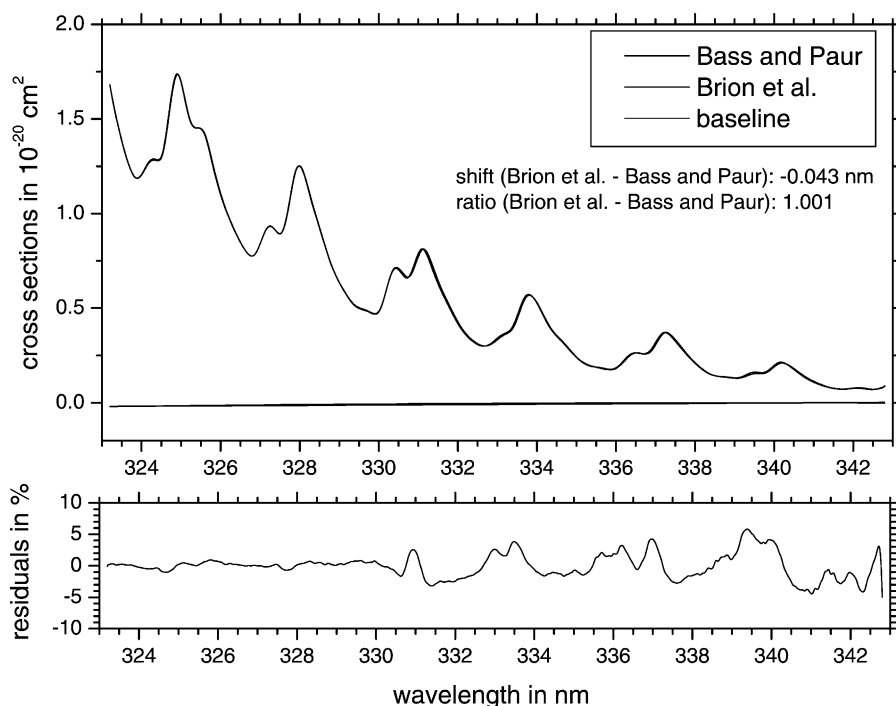


Fig. 7. NLS-fit of O<sub>3</sub> absorption cross-sections at 298 ± 5 K in the Huggins bands (323–343 nm): Bass and Paur compared to Brion et al.

region (323–343 nm) at 298 ± 5 K. It is very important to take into account these systematic differences when comparing O<sub>3</sub> columns determined from the different cross-sections. The results are presented in Table 3. Note that similar comparisons were made for lower temperatures (Section 2.5.3).

*2.5. Comparison of the O<sub>3</sub> cross-sections between 230 and 790 nm at temperatures below room temperature (203–280 K)*

In order to study the absorption cross-sections at temperatures below ambient, we used the same approaches as

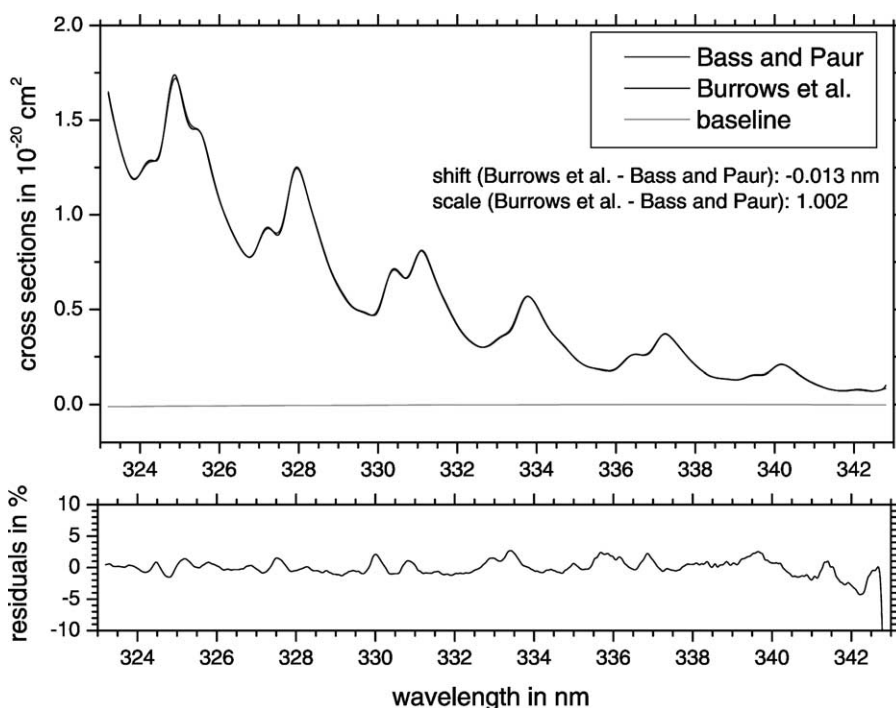


Fig. 8. NLS-fit of O<sub>3</sub> absorption cross-sections at 298 ± 5 K in the Huggins bands (323–343 nm): Bass and Paur compared to Burrows et al.

for the comparisons at room temperature, at four selected temperatures where sufficient laboratory measurements are available:  $276 \pm 4$ ,  $243 \pm 3$ ,  $221 \pm 3$  and  $203 \pm 1$  K.

The following O<sub>3</sub> absorption cross-sections were available in digital form over relatively large spectral intervals:

- Bass and coworkers (245–343 nm) [27,28,33,34];
- Brion and coworkers (300–345 and 515–650 nm) [29–31,43,47,48,52,53];
- Burkholder and Talukdar (407–763 nm) [51];
- Richter et al. (231–794 nm) (unpublished data, 1995);
- Burrows et al. (231–794 nm) [55];
- Voigt et al. (231–851 nm) [60];
- Bogumil et al. (230–1070 nm) [61].

Note that Burkholder and Talukdar [51] and Brion and coworkers [48,52] did not measure O<sub>3</sub> absorption cross-sections at temperatures below 218 K.

### 2.5.1. Relative change of the O<sub>3</sub> absorption cross-sections with temperature

For each set of laboratory cross-sections at different temperatures, the relative change of the O<sub>3</sub> absorption cross-sections with temperature was studied. This approach allows the identification of regions where the effect of temperature is dominant, and reduces systematic errors due to the determination of O<sub>3</sub> amounts during the laboratory measurements.

In the Hartley band (240–310 nm), the cross-sections increase only slightly with decreasing temperature at wavelengths below 260 nm, and start to decrease significantly at lower temperatures at wavelengths above 260 nm. There is agreement between most of the laboratory measurements concerning the “inversion” point around 260 nm and concerning the appearance and amplitude of small periodic features in the ratio between the cross-sections at low and at ambient temperatures. Although there is currently no accurate theoretical prediction for this behaviour, we want to stress the fact that this is basically the same effect as observed upon a small wavelength shift of the absorption cross-sections towards longer wavelengths when the temperature decreases.

In the Huggins bands (310–350 nm), the changes of the cross-sections with decreasing temperature are very strong. Additionally, they depend on the instrumental line shape (e.g. compare the data of Brion et al. and Burrows et al.). The Huggins bands clearly need to be studied independently taking into account the differences in spectral resolution and wavelength calibration (see Section 2.4.3 above and Section 2.5.3 below).

In the Chappuis band (400–790 nm), the available laboratory cross-sections agree in showing very small or no changes of the peak cross-sections (between ca. 550 and 650 nm) with temperature. There is also good agreement concerning the increase of differential structure with decreasing temperature, which shows up as quasi-periodic features in the ratio of the cross-sections. The magnitude of

these features is also in general agreement but needs to be quantified by another method (e.g. non-linear least-squares fits taking into account different baselines, as used for the Huggins bands).

However, there is strong disagreement between the available laboratory cross-sections concerning the relative temperature dependence in the regions 400–550 and 650–790 nm, where the overall temperature dependence is rather irregular except for the cross-sections of Burkholder and Talukdar. The discrepancies between the available absorption cross-sections could be due to baseline problems in different measurements because of the small cross-sections in these regions, but it is difficult to draw conclusions from experimental data with such a large dispersion.

The quasi-period features appearing in the blue and red wings of the Chappuis band (400–550 and 650–790 nm) are clearly visible in all available data. The features are related to an increase in the differential cross-sections of up to 10% between 298 and 203 K. In addition to this differential effect, the band structures between 400 and 500 nm show shifts towards shorter wavelengths with decreasing temperature, see the figures by Burrows et al. and Voigt et al. in the relevant papers. This effect was first observed by Richter et al. and is important for atmospheric retrievals of O<sub>3</sub>.

### 2.5.2. Comparison of the integrated O<sub>3</sub> cross-sections at temperatures below ambient: $276 \pm 4$ , $243 \pm 3$ , $221 \pm 3$ , and $203 \pm 1$ K

As for the cross-sections at room temperature, we have compared the integrated cross-sections since they are rather insensitive to small wavelength shifts and the ILS. Integrated cross-sections were calculated for every temperature in the following spectral regions:

- The Hartley band (245–340 nm).
- The Chappuis band (410–690 nm).
- The Huggins bands (325–340 nm).
- The blue tail of the Chappuis band (410–520 nm).

Note that the latter two windows are currently used for atmospheric O<sub>3</sub> retrieval.

The results are presented in Table 4a–d.

At all temperatures, the agreement of the integrated cross-sections in the Hartley band is better than 2%. The agreement in the Chappuis band is less satisfying, in particular because the integrated cross-sections of Burkholder and Talukdar are systematically below the other measurements by about 3%, and because the data of Burrows et al. are always higher than the other measurements by about 2%. In the Huggins bands, the integrated cross-sections scatter by several percent, indicating systematic differences between the available data, and also in the blue tail of the Chappuis band.

Note that within the experimental uncertainties, the integrated cross-sections of the Hartley and Chappuis bands

Table 4  
Integrated cross-sections of O<sub>3</sub> at different temperatures

Reference	295 ± 3 K	276 ± 4 K	243 ± 3 K	221 ± 3 K	203 ± 1 K
(a) In the Hartley band (245–340 nm) <sup>a</sup>					
Bass and Paur [27,33,34]	3.55	3.54	3.54	3.53	3.52
Brion et al. [30,31,43,47,48,52]	3.52	–	3.50	3.50	–
Richter et al. <sup>b</sup>	3.53	3.49	3.49	3.47	3.47
Burrows et al. [55]	3.57	3.58	3.58	3.56	3.56
Voigt et al. [54,56,60]	3.58	3.57	3.59	3.56	3.56
Bogumil et al. [57–59,61]	3.55	3.56	3.56	3.56	3.56
Average value	3.55	3.55	3.54	3.53	3.53
Relative uncertainty (%)	±0.6	±1.0	±1.1	±1.1	±1.2
(b) In the Huggins bands (325–340 nm) <sup>c</sup>					
Bass and Paur [27,33,34]	8.20	7.27	6.21	5.70	5.44
Brion et al. [30,31,43,47,48,52]	8.32	7.16	6.23	5.65	–
Richter et al. <sup>b</sup>	8.25	7.55	6.28	6.03	5.75
Burrows et al. [55]	8.35	7.73	6.41	6.16	5.93
Voigt et al. [54,56,60]	8.35	7.31	6.18	5.87	5.63
Bogumil et al. [57–59,61]	8.33	7.51	6.46	5.96	5.44
Average value	8.30	7.42	6.30	5.89	5.64
Relative uncertainty (%)	±0.7	±2.9	±1.8	±3.3	±3.7
(c) In the Chappuis band (410–690 nm) <sup>d</sup>					
Burkholder and Talukdar [51]	6.21	6.20	6.17	6.15	–
Brion et al. [53]	6.29	–	–	–	–
Richter et al. <sup>b</sup>	6.47	6.45	6.38	6.29	6.39
Burrows et al. [55]	6.45	6.58	6.44	6.55	6.62
Voigt et al. [54,56,60]	6.42	6.52	6.42	6.45	6.51
Bogumil et al. [57–59,61]	6.41	6.43	6.36	6.33	6.42
Average value	6.38	6.44	6.35	6.35	6.48
Relative uncertainty (%)	±1.6	±2.3	±1.7	±2.4	±1.6
(d) In the blue tail of the Chappuis band (410–520 nm) <sup>c</sup>					
Burkholder and Talukdar [51]	6.35	6.29	6.13	5.99	–
Brion et al. [53]	6.43	–	–	–	–
Richter et al. <sup>b</sup>	7.23	7.00	6.90	6.45	6.79
Burrows et al. [55]	6.75	6.91	6.57	6.55	6.69
Voigt et al. [54,56,60]	6.75	6.77	6.55	6.53	6.67
Bogumil et al. [57–59,61]	6.52	6.57	6.44	6.54	6.68
Average value	6.67	6.71	6.52	6.41	6.71
Relative uncertainty (%)	±4.8	±4.2	±4.3	±3.7	±0.8

<sup>a</sup> The integrated cross-sections are given in units of 10<sup>-16</sup> cm<sup>2</sup> × nm.

<sup>b</sup> Unpublished values based on the data of [55].

<sup>c</sup> The integrated cross-sections are given in units of 10<sup>-20</sup> cm<sup>2</sup> × nm.

<sup>d</sup> The integrated cross-sections are given in units of 10<sup>-19</sup> cm<sup>2</sup> × nm.

remain constant in the temperature range considered, with less accuracy however for the Chappuis band.

### 2.5.3. Non-linear least-squares fits of the O<sub>3</sub> cross-sections in the Huggins bands at temperatures below ambient: 276 ± 4, 243 ± 3, 221 ± 3, and 203 ± 1

As already explained above (Section 2.4.3), the cross-sections in the Huggins bands were compared using a non-linear least-squares fitting approach. The results from the non-linear least-squares fits are summarized in Table 5a and b.

At all temperatures including room temperature, the cross-sections of Burrows et al. are the highest, followed by the data of Bass and Paur, Brion et al., and Richter

et al. The cross-sections of Voigt et al. and of Bogumil et al. seem to be influenced by baseline drifts (as also observed when comparing the relative temperature dependence, see above). At all temperatures where data are available, the agreement between the cross-sections of Bass and Paur and Brion et al. is good (better than 0.5%), and both sets of data need only small baseline corrections.

Concerning the wavelength shifts, the results at lower temperatures confirm the observations at room temperature: the wavelength scale of Brion et al. is slightly non-linear, and high-order shift-and-squeeze is required for an agreement of better than 0.01 nm. The data of Bass and Paur need significant wavelength shifts of 0.03–0.05 nm.

Table 5

(a) Relative differences in the cross-sections of O<sub>3</sub> at different temperatures in the Huggins bands (323–343 nm) and (b) wavelength shifts (in nm) in the cross-sections of O<sub>3</sub> at different temperatures in the Huggins bands (323–343 nm)

Reference 1	Reference 2	295 K	273 K	243 K	223 K	203 K
(a) Relative differences						
–	Bass and Paur [27,33,34]	1.000	1.000	1.000	1.000	1.000
Bass and Paur [27,33,34]	Brion et al. [47,48,52]	1.001	0.998	0.995	0.992	–
Bass and Paur [27,33,34]	Voigt et al. [54,56,60]	0.956	1.040	1.063	1.079	1.195
Bass and Paur [27,33,34]	Richter et al. <sup>a</sup>	1.014	1.013	1.016	1.018	1.011
Bass and Paur [27,33,34]	Burrows et al. [55]	1.002	0.989	0.992	0.995	0.983
Bass and Paur [27,33,34]	Bogumil et al. [57–59,61]	1.049	1.050	1.065	1.080	1.077
(b) Wavelength shifts						
–	Bass and Paur [27,33,34]	0.000	0.000	0.000	0.000	0.000
Bass and Paur [27,33,34]	Brion et al. [47,48,52]	–0.043	–0.027	–0.022	–0.026	–
Bass and Paur [27,33,34]	Voigt et al. [54,56,60]	–0.029	–0.030	–0.032	–0.037	–0.047
Bass and Paur [27,33,34]	Richter et al. <sup>a</sup>	–0.013	–0.007	–0.007	–0.012	–0.015
Bass and Paur [27,33,34]	Burrows et al. [55]	–0.013	–0.007	–0.007	–0.012	–0.015
Bass and Paur [27,33,34]	Bogumil et al. [57–59,61]	–0.015	–0.014	–0.017	–0.025	–0.021

<sup>a</sup> Unpublished values based on the data of [55].

## 2.6. Empirical models for the temperature-dependence of the O<sub>3</sub> cross-sections in the 240–790 nm region

First, we want to point out that from the results of Section 2.5.2, we concluded that the integrated cross-sections change only significantly in the region of the Huggins bands. This is consistent with the Born–Oppenheimer approximation which is applicable for O<sub>3</sub> since there is no low-lying electronic state that couples the electronic and vibrational wavefunctions for energies corresponding to the temperature range that is considered here 202–300 K. In the Huggins bands, however, the integrated cross-sections become lower with decreasing temperature due to the decreasing absorption of the “red” tail of the Hartley band.

Second, it was concluded that there are relative changes of the spectrum which are observed in the peak region of the Hartley band, in the Huggins bands, and in the Chappuis band. These changes are strongest in the Huggins bands.

The most difficult region is therefore the region of the Huggins bands where two effects are present: an overall decrease of the cross-sections together with strong changes in the differential structure of the bands.

Generally, three different models have been proposed in the past to reproduce the temperature-dependence of the absorption cross-sections of O<sub>3</sub>.

- The first model [Adler–Golden] uses an exponential function:

$$\frac{\sigma(\lambda, T)}{\sigma(\lambda, T_0)} = c_1(\lambda) \times \exp\left[-\frac{1300}{T}\right] + c_2(\lambda)$$

where  $T$  is the temperature in K,  $T_0$  is 295 K, and  $c_1(\lambda)$  and  $c_2(\lambda)$  the wavelength-dependent coefficients. The factor 1300 in the exponential term arises from the Boltzmann factor for a vibrational energy of 900 cm<sup>–1</sup> which is close to the average energy of the  $n_1$ ,  $n_2$ , and  $n_3$  vibrations of ozone in the electronic ground state. This model was

only applied to the temperature-dependence of the O<sub>3</sub> absorption cross-sections in the Hartley band.

- The second model [Bass and Paur] use a quadratic polynomial:

$$\frac{\sigma(\lambda, T)}{\sigma(\lambda, T_0)} = c_0(\lambda) + c_1(\lambda) \times T + c_2(\lambda) \times T^2$$

where  $T$  is the temperature in K and  $c_0(\lambda)$ ,  $c_1(\lambda)$ , and  $c_2(\lambda)$  the wavelength-dependent coefficients. Although there is no physical interpretation of this model it was concluded by several authors in the past that this function can reproduce the temperature-dependence of the O<sub>3</sub> absorption cross-sections within the experimental uncertainties, even in the Huggins bands.

- The third model [Voigt et al.] uses a double exponential function:

$$\frac{\sigma(\lambda, T)}{\sigma(\lambda, T_0)} = \frac{c_0(\lambda)}{\lambda} \times \exp\left[\frac{-c_1(\lambda)}{T} + c_2(\lambda) \times T\right]$$

where  $T$  is the temperature in K and  $c_0(\lambda)$ ,  $c_1(\lambda)$ , and  $c_2(\lambda)$  the wavelength-dependent coefficients. The latter coefficients are proportional to the temperature-independent transition moment and to the Boltzmann factor of the lower states involved in the transitions.

We have investigated the accuracy of the three models using the experimental data of Richter et al. in the entire region between 240 and 790 nm). Before the calculations, the experimental data at five temperatures were interpolated to a new grid with a spacing of 0.1 nm.

We have observed that the exponential models are both very sensitive to baseline uncertainties, so that the experimental data are better reproduced using a quadratic polynomial. The latter reproduced the experiments to better than 1%.

In the absence of any theoretical model for the temperature-dependence of the O<sub>3</sub> cross-sections, it is therefore

recommended to use a quadratic polynomial to interpolate the experimental data for intermediate temperatures.

### 3. Nitrogen dioxide

#### 3.1. The $\text{NO}_2$ absorption spectrum in the 240–790 nm region

The  $\text{NO}_2$  absorption cross-sections in the 240–790 nm region (see Fig. 9) can be separated into two principal systems: the D–X band system below 250 nm and the broad B–X and A–X band systems between 300 and 790 nm, with a maximum at around 400 nm (see Fig. 13); due to interactions the forbidden C–X transition can also contribute to the

visible spectrum of  $\text{NO}_2$ . The shape of the visible system is a close to a Gaussian function, but there is a lot of spectral fine structure superimposed on it (see Fig. 10). Due to the complexity of the excited electronic states of  $\text{NO}_2$ , it is impossible to predict its spectrum from molecular quantum theory within experimental accuracy.

The dissociation energy of  $\text{NO}_2$  is about  $25,000 \text{ cm}^{-1}$  (400 nm) but there has been observation of dissociation products already at slightly lower energies. At energies above  $25,000 \text{ cm}^{-1}$  (wavelengths below 400 nm) the fine structure of the spectrum becomes larger due to lifetime broadening (see Fig. 11). The density of energy levels of  $\text{NO}_2$  in the UV-Vis is very high, in particular when approaching the dissociation limit (hundreds to thousands of states per  $\text{cm}^{-1}$ ). Furthermore, the strong coupling between

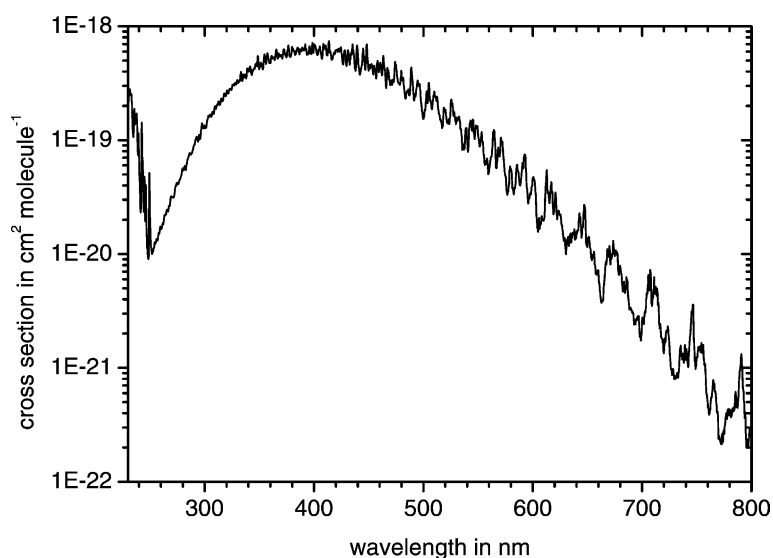


Fig. 9. The  $\text{NO}_2$  spectrum at room temperature (source: [57–59,61,92,93]).

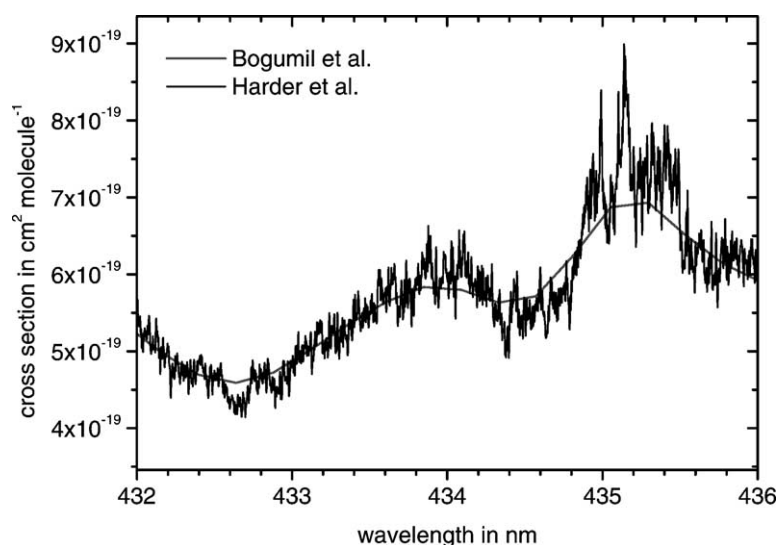


Fig. 10. The  $\text{NO}_2$  cross-sections at high spectral resolution (source: [84]).

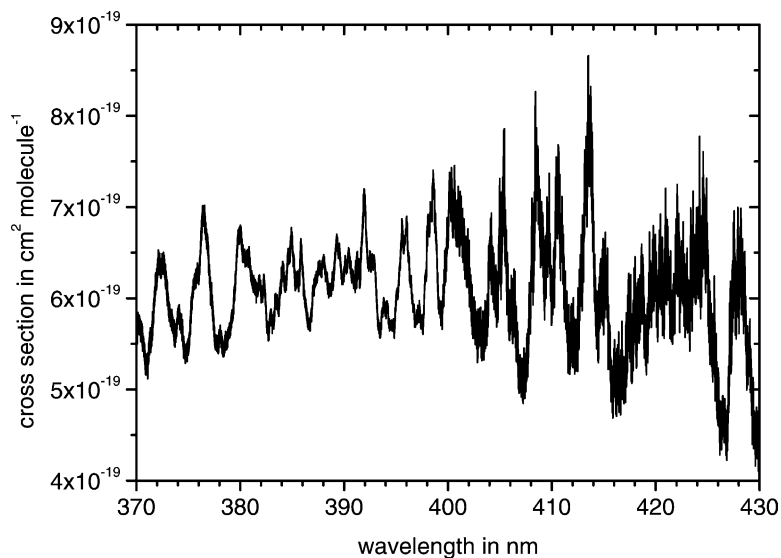


Fig. 11. Lack of spectral fine-structure in the  $\text{NO}_2$  cross-sections below 400 nm due to dissociation (lifetime broadening) at high spectral resolution (source: [84]).

the ground and first excited electronic states leads to a large number of optically active transitions that causes the irregular structure of the bands.

The spectral width of these features is limited by the density of lines and by the Doppler broadening due to thermal motion of the molecules: the Doppler linewidth (at 300 K) is varying slowly from  $0.023 \text{ cm}^{-1}$  at  $12,658 \text{ cm}^{-1}$  (i.e.  $0.0014 \text{ nm}$  at  $790 \text{ nm}$ ) to  $0.045 \text{ cm}^{-1}$  at  $25,000 \text{ cm}^{-1}$  (i.e.  $0.0007 \text{ nm}$  at  $400 \text{ nm}$ ). At higher energies (i.e. at lower wavelengths) the spectral structures become rapidly larger because of the limited lifetime of the upper states due to the  $\text{NO}_2$  dissociation mentioned above.

At higher total pressures, collisional broadening can be observed (see Fig. 12). In the limit of isolated spectral lines, the collisional broadening leads to a Lorentzian lineshape with a linewidth that augments linear proportionally to the total pressure. Typical values for this linewidth are of the order of  $0.1 \text{ cm}^{-1} \text{ atm}^{-1}$  (i.e.  $0.0062 \text{ nm}$  at  $790 \text{ nm}$  and  $0.0016 \text{ nm}$  at  $400 \text{ nm}$ ). Obviously, very high spectral resolution is required to observe these pressure effects.

In the entire region, the cross-sections also vary with the absolute temperature, see Fig. 13. At low temperatures, the differential structure is significantly stronger.

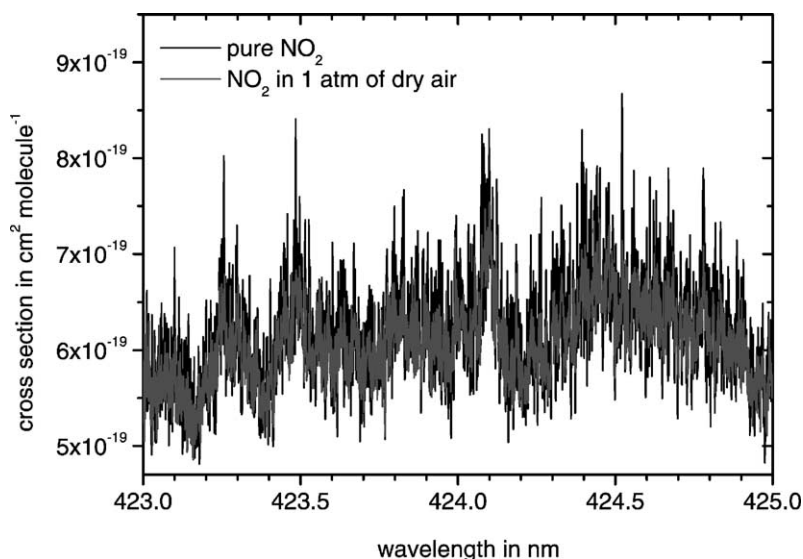


Fig. 12. Pressure-broadening of the  $\text{NO}_2$  cross-sections at foreign pressures of zero and one atmosphere at high spectral resolution (source: Vandaele et al., 2002).

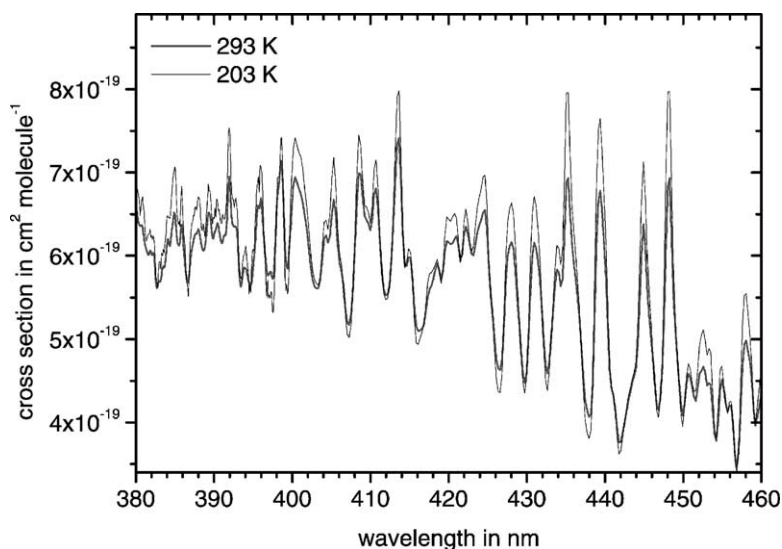


Fig. 13. The  $\text{NO}_2$  cross-sections at 293 and 203 K (source: [57–59,61,92,93]).

Unfortunately, there have been no measurements of absolute absorption cross-sections of  $\text{NO}_2$  at very high spectral resolution ( $0.02 \text{ cm}^{-1}$  or better) in the entire region of interest (250–790 nm). We were therefore limited to compare laboratory absorption cross-sections at spectral resolutions that are limited by the instrumental techniques employed and not by the absorber itself [64–98]. Due to the non-commutability of convolution (that occurs on the transmission spectra) and the logarithm (that is used to transform the transmission spectra into absorption cross-sections) the different laboratory spectra show differences due to the unresolved spectral structures.

In the last years, several sets of very high-resolution measurements of  $\text{NO}_2$  cross-sections have been published by different groups [79,80,82–84,86–89,91,94–98]. In earlier times, the cross-section measurements were however limited to lower spectral resolution [64–78], because the authors believed that it was sufficient to use low-resolution spectra, for example here:

*“In a previous work . . . we had measured the absorption cross-sections of  $\text{NO}_2$  at two different temperatures 298 and 235 K, but only for the consecutive maxima and minima in the 426.8–449.9 nm range. We have taken up again this work in order to obtain these absorption cross-sections for the same spectral range but detailing the complete cross-sections at steps of 0.1 nm.*

*The following reasons have led us to complete the previous results:*

*An absorption measurement is always made with a finite spectral resolution which determines the slit function of the instruments which has been used. The result of the measurement is the convolution product of the real spectrum by the slit function . . . . The absorption cross-section cannot be considered as a constant in the spectral range defined by the instrument. Consequently, to determine precisely the*

*convolution product it is necessary to obtain absorption cross-section values at narrow wavelength intervals. The strict application of Boguer–Beer–Lambert’s absorption law would lead to an incorrect value of the absorbing component’s optical thickness.*

*Furthermore, there is a need for tabulated results with a finer wavelength interval resolution; for example for the data analysis of the MAP GLOBUS I and II campaigns.”* (Source: Leroy et al. [70]).

Today, it is generally agreed that the absorption cross-sections must be recorded at highest resolution to avoid instrumental limitations: even if the logarithm can be approached with a linear development (at small optical densities, e.g. 0.01 or less) as is often the case for atmospheric  $\text{NO}_2$  retrievals, the laboratory cross-sections have always been recorded at higher optical densities (0.1–1.0) so that the convolution still leads to a deformation of the spectra. This can then limit the detection of other weak absorbers due to residual features.

It is a difficult question how to compare laboratory measurements that have been obtained using different instruments and experimental conditions, in particular because all available cross-sections of  $\text{NO}_2$  are still limited by instrumental effects. In the following sections, several approaches that have been used for these comparisons are presented: absolute values over large regions (also after convolution of high-resolution cross-sections to those at lower resolution) to investigate baseline problems, integrated cross-sections, and non-linear least-squares fits to account for wavelength calibration errors.

### 3.2. Sensitivity of the $\text{NO}_2$ cross-sections to wavelength shifts and resolution

In the previous sections, we have concluded that the spectral structures of  $\text{NO}_2$  have intrinsic widths of at least

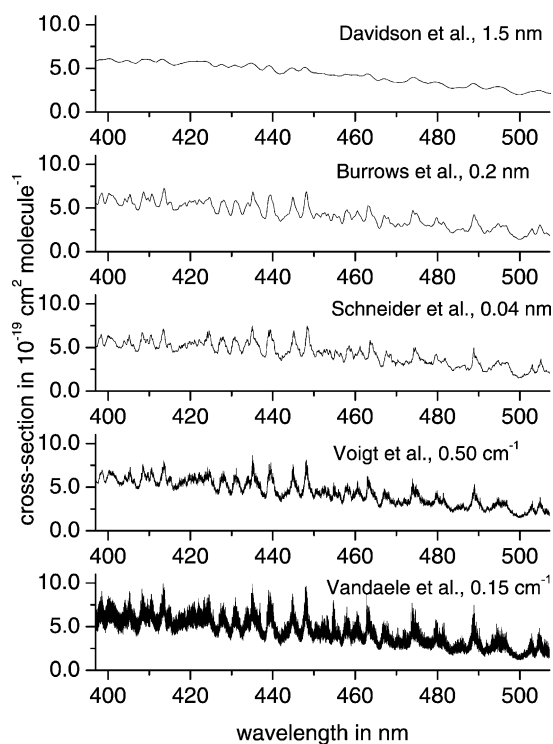


Fig. 14. Change of  $\text{NO}_2$  cross-sections in the 400–500 nm region at different spectral resolutions (note:  $0.5 \text{ cm}^{-1}$  correspond to  $0.008 \text{ nm}$  at  $400 \text{ nm}$ , and  $0.15 \text{ cm}^{-1}$  to  $0.0024 \text{ nm}$ ).

$0.023\text{--}0.045 \text{ cm}^{-1}$  ( $0.0014\text{--}0.0007 \text{ nm}$ ) between  $12,658$  and  $25,000 \text{ cm}^{-1}$  ( $790$  and  $400 \text{ nm}$ ). The cross-sections can therefore be sensitive to spectral resolutions even at ca.  $0.02 \text{ cm}^{-1}$ . The available laboratory data with highest resolution are however limited to about  $0.1 \text{ cm}^{-1}$  (corresponding to  $0.0016 \text{ nm}$  at  $400 \text{ nm}$  and to  $0.0062 \text{ nm}$  at  $790 \text{ nm}$ ) which is insufficient for such an investigation (see Fig. 14). The cross-sections will probably start to become entirely insensitive to spectral resolution at instrumental linewidths below  $0.01 \text{ cm}^{-1}$ , a resolution that has not yet been used. In any case, the  $\text{NO}_2$  cross-sections are very sensitive to small wavelength shifts at high resolution. The influence of spectral shifts becomes however less significant at lower spectral resolution.

It is important to stress the fact that, since relative changes were studied, the differing absolute values of the cross-sections and the wavelength calibration errors in the experimental data do not show up in these comparisons.

At spectral resolutions of  $0.2 \text{ nm}$  or less, the  $\text{NO}_2$  cross-sections change by  $2\text{--}7\%$  after wavelength shifts of  $0.05 \text{ nm}$  and by  $<2\%$  after wavelength shifts of  $0.01 \text{ nm}$ , in the region  $250\text{--}790 \text{ nm}$ . Between  $400$  and  $500 \text{ nm}$  (an important region for ground-based remote-sensing), the cross-sections change by  $<5\%$  for wavelength shifts of  $0.05 \text{ nm}$  and by  $<1\%$  for wavelength shifts of  $0.01 \text{ nm}$ , at spectral resolution of  $0.2 \text{ nm}$  or less. At high spectral resolution ( $0.10\text{--}0.15 \text{ cm}^{-1}$ ), the  $\text{NO}_2$  absorption cross-sections

change by a few tens up to several hundred percent in the region  $250\text{--}790 \text{ nm}$ , even for shifts of only  $0.01 \text{ nm}$ .

In the region  $400\text{--}500 \text{ nm}$ , the changes are  $20\text{--}100\%$  for shifts of  $0.01 \text{ nm}$  for spectral resolutions ranging from  $0.10$  to  $0.50 \text{ cm}^{-1}$ .

The changes are always highest towards the near-infrared, probably due to the lower spectral congestion (less separated transitions per spectral interval).

There is an increase of noise towards lower wavelengths in all the high-resolution cross-sections [42,49,54,60,83,84,86,88,89,94–98].

Below  $400 \text{ nm}$ , there is a sudden drop in the sensitivity of the  $\text{NO}_2$  absorption cross-sections to spectral shifts (see, for example, Figs. 15 and 16). Even at high resolution (i.e.  $0.10\text{--}0.15 \text{ cm}^{-1}$ ) the cross-sections change by  $<5\%$  for shifts of  $0.05 \text{ nm}$ . This observation can be attributed to the intrinsic broadening of the  $\text{NO}_2$  spectral features below  $400 \text{ nm}$  due to the limited lifetime of the upper states.

Obviously, when we compare  $\text{NO}_2$  absorption cross-sections at high resolution (ca.  $0.1 \text{ nm}$  or better) in the region above  $400 \text{ nm}$ , the wavelength scale of the different laboratory data must agree very well (i.e. better than  $0.01 \text{ nm}$ ). At lower resolution (ca.  $0.2 \text{ nm}$  or less), a wavelength accuracy of about  $0.01 \text{ nm}$  is sufficient to reduce the systematic error due to wavelength calibration errors to  $<0.5\%$  below  $500 \text{ nm}$  and to  $<2\%$  above  $500 \text{ nm}$ .

Clearly, it is not useful to compare the  $\text{NO}_2$  cross-sections at single wavelengths, due to their strong dependence on spectral resolution and wavelength accuracy.

For atmospheric remote-sensing, the wavelength calibration of the field instruments must agree very well with those of the laboratory cross-sections. It is, however, difficult to achieve a wavelength accuracy of better than  $0.01 \text{ nm}$  with the grating instruments currently used for recording atmospheric spectra (spectral resolutions of about  $0.1\text{--}0.5 \text{ nm}$ ).

### 3.3. Comparison of the $\text{NO}_2$ cross-sections between $230$ and $790 \text{ nm}$ at $295 \pm 3 \text{ K}$

#### 3.3.1. Comparison of room temperature cross-sections over large regions

When comparing the cross-sections over large regions, systematic differences between the available laboratory cross-sections are observed:

- The data show large differences in the region above  $400 \text{ nm}$  probably due to the different spectral resolutions employed and also due to wavelength calibration errors in some of the data.
- The data often show noise on the edges of the data set, probably because the signal of the broad-band sources used for the experiments had lower output in these regions.
- High-resolution cross-sections are difficult to compare in the region above  $400 \text{ nm}$  due to the large differences in spectral resolution.
- The cross-sections by Burrows and coworkers (GOME-FM) are systematically  $6\text{--}8\%$  lower than the most recent

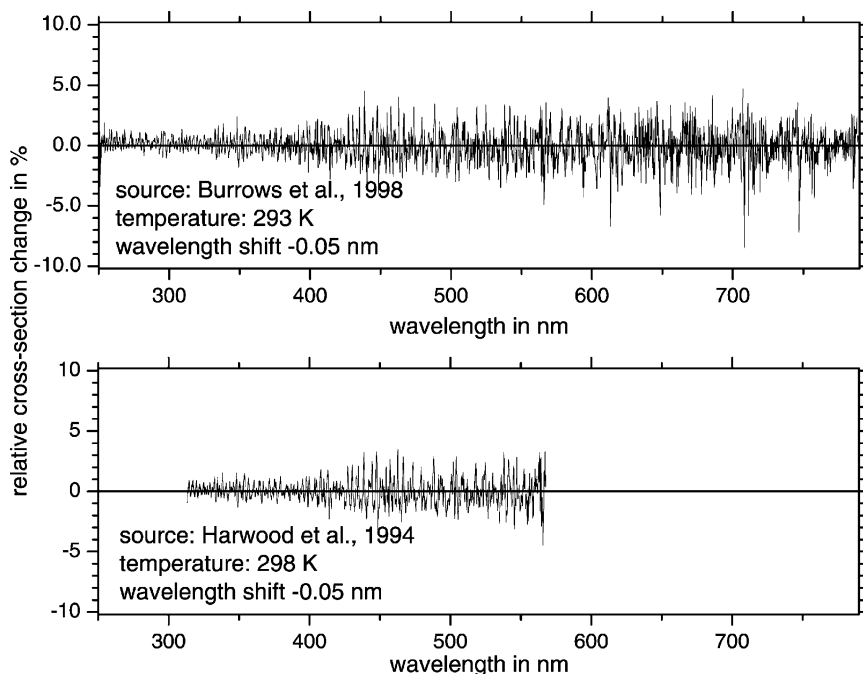


Fig. 15. Change of NO<sub>2</sub> cross-sections ([7,8,55,90], spectral resolution ca. 0.2–0.4 nm and Harwood et al., spectral resolution 0.54 nm) after a wavelength shift of  $-0.01$  nm.

high-resolution cross-sections [54,60,79,83,84,87–89, 94–98].

- The high-resolution cross-sections convoluted down to 0.2 nm FWHM agree within 5% between 300 and 400 nm and within 7% in the region 400–500 nm. Above 500 nm

and below 300 nm, the differences are larger, probably due to the influence of baseline (lamp) drifts in the regions of small cross-sections.

- There are systematic high-frequency differences in the high-resolution cross-sections convoluted down to 0.2 nm

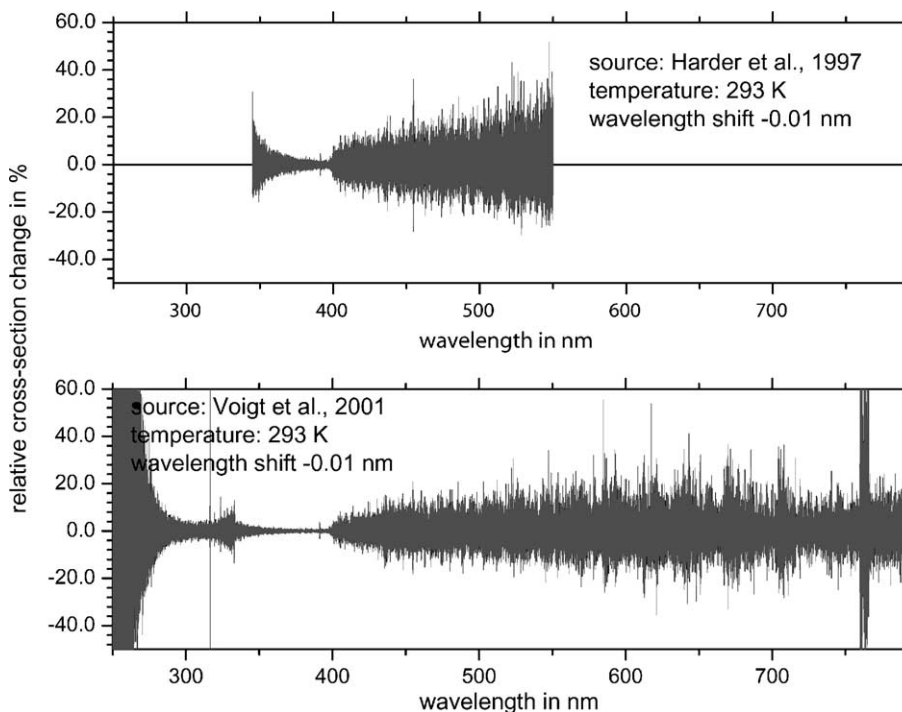


Fig. 16. Relative change of NO<sub>2</sub> cross-sections ([84], spectral resolution 0.15 cm<sup>-1</sup> and [54,56,60,89,91,96], spectral resolution 0.50 cm<sup>-1</sup>) after a wavelength shift of  $-0.01$  nm.

HWHM. These differences are of the order of 0.5–2.0% and are probably due to remaining differences in the instrumental lines shapes of the initial high-resolution cross-sections and possibly to the non-commutability of the natural logarithm and the convolution operations. This indicates that an agreement of better than 1% is difficult to achieve, even when comparing very high resolution cross-sections convoluted with a broad smoothing function or instrumental line shape.

- Very often there are broad-band low-frequency differences of several percent different from simple scaling factors, probably due to lamp drifts between the empty-cell reference spectra and the absorption spectra with NO<sub>2</sub> in the cell (for example, a clear tilt in the cross-sections of Harder et al. towards longer wavelengths and large structures around 500 nm in the data of Voigt et al).
- There are systematic differences (offsets in the relative differences) that are probably due to differences in the determination of the NO<sub>2</sub> amounts in the absorption cell.

In the following chapter, we will summarize what previous authors concluded concerning the comparison of their cross-sections with those published earlier.

### 3.3.2. Comparisons of NO<sub>2</sub> cross-sections at room temperature by other authors

In the past years, some authors have made comparisons of previously published laboratory cross-sections of NO<sub>2</sub> at room temperature.

- Harder et al. [84];
- Vandaele et al. [88];
- Vandaele et al. [97,98].

The following conclusions were drawn by these authors:

Harder et al. [84] showed that in the 400–600 nm region, the cross-sections of Johnston and Graham agree within 0.5% with their data after a few simple operations (wavelength shifts and baseline corrections). The same authors showed that the cross-sections by Schneider et al. have a baseline error leading to lower cross-sections in large regions of the spectrum and some serious wavelength errors. They also found a correction factor of 1.08 between the cross-sections of Davidson et al. and their own data in the region 350–585 nm, after some operations (detector blooming correction and wavelength correction). In addition they showed that the data of Harwood and Jones are 7–14% lower than the new cross-sections in the 350–550 nm region and that the cross-sections of Harwood and Jones show some periodic baseline errors. Finally, they pointed out that there are undersampling problems in the cross-sections by Merienne et al. (spectral resolution 0.01 nm, data sampled in steps of 0.01 nm) and by Bass et al. (spectral resolution 0.015–0.04 nm, data sampled in steps of 0.125 nm), and they determined a correction factor of 1.04 to bring the data of Merienne

et al. in agreement with their new cross-sections in the 350–500 nm region.

Vandaele et al. [88] found an agreement of  $\pm 1.5\%$  between their new data and those of Merienne et al. They observed that the cross-sections by Yoshino et al. are about 2% lower than their new data. They also observed small wavelength shifts in the data by Yoshino et al. The same authors give a relative difference of their new cross-sections to the data of Bass et al. of +3% (cross-sections below 410 nm), of +6% compared to the data of Harwood and Jones, and of –2% to the cross-sections of Johnston and Graham.

Vandaele and coworkers [97,98]. Using the new cross-sections, these authors found an agreement of 2.5% between their new data and those published in Vandaele et al. [88]. They observed an agreement of 1.9% between their new data and those of Merienne et al., and – below 500 nm – of 3.0% with the cross-sections of Harder et al. Above 500 nm, the cross-sections of Harder decrease up to –5% compared to the new data of Vandaele and coworkers [97,98]. Between 400–500 nm, the agreement with the cross-sections of Voigt et al. is on average better than 5%, but there are large parasitic features in the latter data around 500 nm (compare with Figs. 15–19).

All these conclusions are in good agreement with the observations in the figures below and with the conclusions on the previous pages, except those by Vandaele and coworkers [97,98] concerning their new cross-sections (which are probably slightly too low at the highest pressure).

### 3.3.3. Integrated NO<sub>2</sub> absorption cross-sections at room temperature

Because integrated absorption cross-sections are rather insensitive to differences in small spectral intervals, we have calculated these values for the following regions:

- For the region 400–500 nm, because most of the available cross-sections cover this region and because this window is very important for remote-sensing.
- For the region 400–450 nm, because this also includes the data of Yoshino et al. and limits the region to the strongest cross-sections where the influence of baseline errors should be smaller than elsewhere.

When available, we have used the NO<sub>2</sub> cross-sections at atmospheric pressure.

The results are given in Table 6. One can state that the agreement between the different data is better than 2.4% for the region 400–500 nm. The most recent data of Merienne et al., Vandaele et al. [83], Harder et al., Vandaele et al. (1997), Voigt et al., and Vandaele and coworkers [97,98] yield a mean value of  $4.52 \times 10^{-17} \text{ cm}^2 \times \text{nm}$  with a standard deviation of 1.5%.

In the reduced region 400–450 nm, a similar result is obtained: all different laboratory measurements agree within 2.6% ( $1\sigma$ ). Note that baseline errors can also cancel out some

Table 6  
Integrated absorption cross-sections of NO<sub>2</sub><sup>a</sup> at 295 ± 3 K

Reference	400–500 nm	400–450 nm
Hall and Blacet [65] <sup>b</sup>	$4.54 \times 10^{-17}$	$2.78 \times 10^{-17}$
Schneider et al. [73]	$4.42 \times 10^{-17}$	$2.66 \times 10^{-17}$
Johnston and Graham [66]	$4.72 \times 10^{-17}$	$2.91 \times 10^{-17}$
Davidson et al. [74]	$4.47 \times 10^{-17}$	$2.76 \times 10^{-17}$
Harwood and Jones [78]	$4.34 \times 10^{-17}$	$2.68 \times 10^{-17}$
Merienne et al. [79,80,82,87]	$4.55 \times 10^{-17}$	$2.81 \times 10^{-17}$
Vandaele et al. [83]	$4.52 \times 10^{-17}$	$2.79 \times 10^{-17}$
Harder et al. [84]	$4.60 \times 10^{-17}$	$2.85 \times 10^{-17}$
Vandaele et al. [88]	$4.58 \times 10^{-17}$	$2.83 \times 10^{-17}$
Yoshino et al. [86]	–	$2.76 \times 10^{-17}$
Burrows et al. [90]	$4.33 \times 10^{-17}$	$2.68 \times 10^{-17}$
Voigt et al. [89,91,96]	$4.48 \times 10^{-17}$	$2.76 \times 10^{-17}$
Bogumil et al. [57–59,61]	$4.58 \times 10^{-17}$	$2.84 \times 10^{-17}$
Vandaele et al. [94,95,97,98]	$4.41 \times 10^{-17}$	$2.72 \times 10^{-17}$
Average value	$4.50 \times 10^{-17}$	$2.77 \times 10^{-17}$
Standard deviation (1σ) (%)	±2.4	±2.6

<sup>a</sup> The integrated cross-sections are given in units of cm<sup>2</sup> × nm.

<sup>b</sup> From the digital data available, a value of  $4.87 \times 10^{-17}$  cm<sup>2</sup> × nm was obtained. But the authors do not specify whether the extinction coefficient (in cm<sup>-1</sup> mm<sup>-1</sup> Hg) is given for 273 or for 293 K. When applying a correction of  $(T/T_0) = 293/273 = 1.073$ , one gets the more probable value  $4.54 \times 10^{-17}$  cm<sup>2</sup> × nm.

systematic errors, e.g. errors in the determination of the NO<sub>2</sub> concentration during the experiments. It is, therefore, interesting to perform comparison of the NO<sub>2</sub> cross-sections using non-linear least squares fits (including wavelength shifts, baseline errors, and a scaling factor).

### 3.3.4. Comparison of the NO<sub>2</sub> cross-sections using non-linear least squares fits

Because of the importance of small wavelength shifts and of the spectral resolution, we have used the following procedure, in the region 390–460 nm:

- All recent high-resolution cross-section spectra were convoluted with a Gaussian with a 0.4 nm FWHM
- These spectra were then compared with a non-linear least-squares fitting program, with five fitting parameters: a quadratic baseline polynomial (i.e. three parameters), a scaling coefficient for the magnitude of the cross-sections (one parameter), and a linear wavelength shift coefficient (one parameter).

The convolution is employed to minimize the influence of spectral resolution when comparing cross-sections recorded at rather high resolution (i.e. [42,49,54,60,79,83,84,86–89,94–98]).

The non-linear least-squares fitting program is employed to minimize the influence of wavelength shifts and of baseline drifts or straylight. We have verified that the convolution does not change the scaling and shifting parameters within the experimental uncertainties.

The region 390–460 nm was selected because the cross-sections are strongest here, and because this region is important for atmospheric remote sensing of NO<sub>2</sub> and of

other trace gases (O<sub>3</sub>, BrO, OClO, IO). The cross-sections of Vandaele and coworkers [97,98] start at 387 nm and the cross-sections of Yoshino et al. end at 468 nm. In order to use the same spectral region, we limited the fits to the range that is common to all recent high-resolution cross-section measurements.

Note that some of the remaining residuals arise from using only a linear shift term (in particular for the grating spectrometer data of Merienne et al. and Yoshino et al.).

From the fits (see, for example, Figs. 17 and 18), one can draw the following conclusions:

- The NO<sub>2</sub> cross-sections from the different experiments show deviations of up to 5% concerning the magnitude of the NO<sub>2</sub> cross-sections between 390 and 460 nm, after correction for baseline effects and wavelength shifts.
- The remaining residuals are in the order of 2–5%, and are due to non-linear wavelength differences (we used only a linear shift), to the differences in the ILS of the laboratory spectra, and partly also to the non-linearity of the convolution.
- Most of the data except for that of Voigt et al. show only very small baseline differences.
- The data of Merienne et al., Vandaele et al. [83], Harder et al., Yoshino et al., and Vandaele et al. [88] show very good agreement concerning the magnitude of the cross-sections: the relative difference between Merienne et al. and Vandaele et al. [88] is 0.5%, the relative difference between Vandaele et al. [83] and Vandaele et al. [88] is 0.2%, the relative difference between Harder et al. and Vandaele et al. [88] is 1.0%, and the relative difference between Yoshino et al. and Vandaele et al. [88] is 1.4%.
- The data of Vandaele et al. [83], Vandaele et al. [88], and Vandaele and coworkers [97,98] show small but systematic wavelength differences, but agree very well between each other with respect to wavelength calibration.
- The data of Voigt et al. are smaller than the cross-sections of Vandaele et al. [88] by about 6.5%. The high-pressure cross-sections of Vandaele et al. (2001) are smaller than the values of Vandaele et al. [88] by about 3.7%.
- The data of Vandaele and coworkers [97,98] seem to contain noise of the order of a few percent (increasing towards smaller wavelengths). Here, pressure effects are excluded because the cross-sections of Voigt et al. were also recorded at high total pressure. Resolution effects can also be ruled out because the cross-sections of Harder et al. and Yoshino et al. were recorded at similar resolutions.
- The overall wavelength accuracy is very good, i.e. 0.001 nm and better.

Using the relative differences obtained from the non-linear least-squares fits (see Table 7), we have determined the relative differences of each individual spectrum to the average

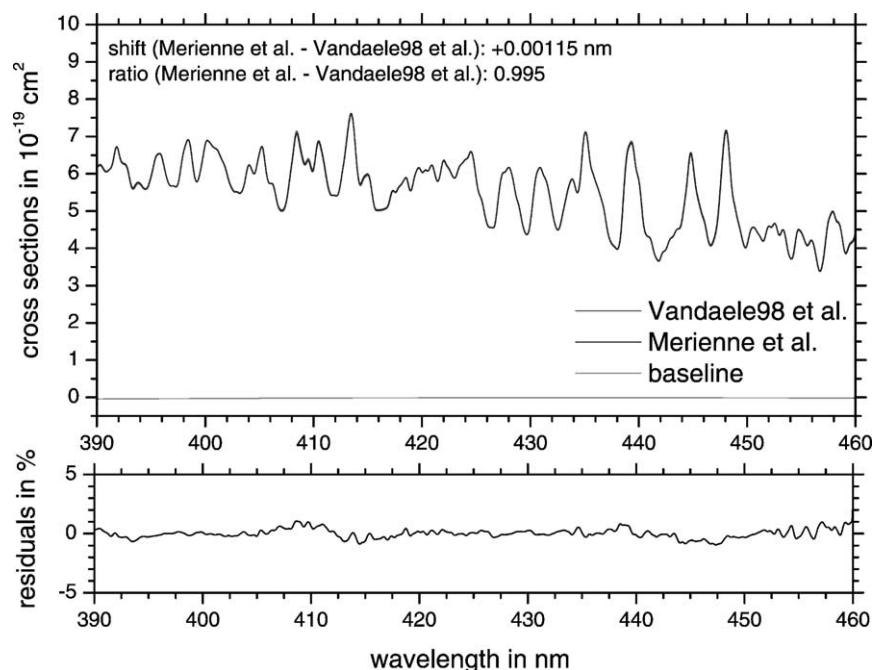


Fig. 17. NLS-fit of  $\text{NO}_2$  absorption cross-sections at  $295 \pm 3$  K in the 390–460 nm region: Merienne et al. compared to Vandaele et al. [88].

values (taking into account the different wavelength shifts and the baseline differences) for the  $\text{O}_3$  cross-sections in this region (323–343 nm) at  $298 \pm 5$  K.

Note that the data by Vandaele et al. [83,88,97,98] agree very well between each other with respect to wavelength calibration, but that all other independent data

[42,49,54,60,79,84,86,87,89,96] indicate that there is a small wavelength calibration error of about 0.0012 nm in the data of Vandaele et al.

Except for the cross-sections by Voigt et al. and by Vandaele and coworkers [97,98], all other data agree within <1.5%.

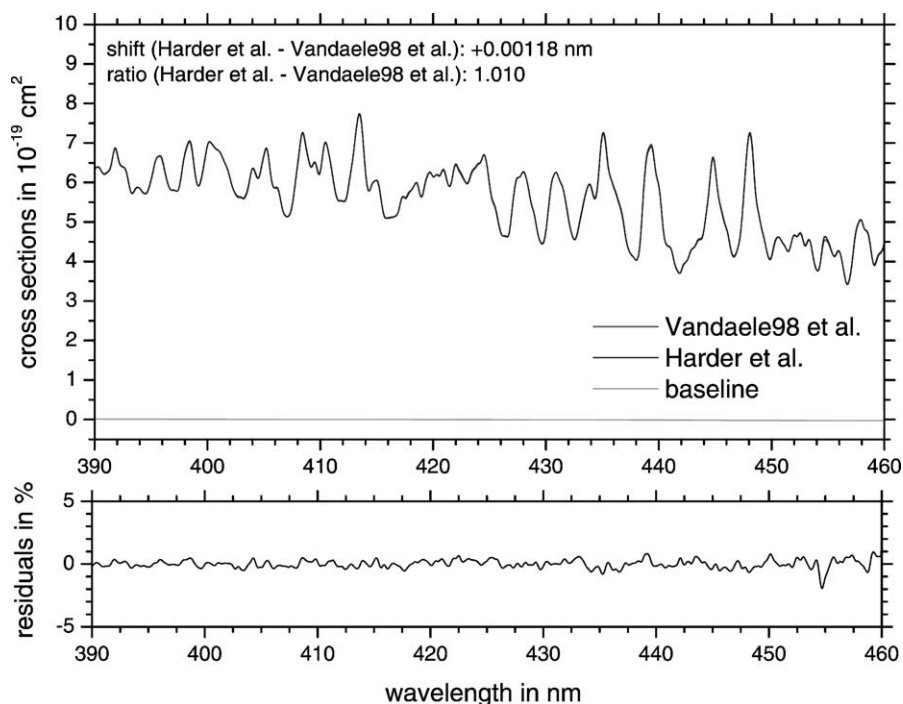


Fig. 18. NLS-fit of  $\text{NO}_2$  absorption cross-sections at  $295 \pm 3$  K in the 390–460 nm region: Harder et al. [84] compared to Vandaele et al. [88].

Table 7

Comparison of NO<sub>2</sub> cross-sections at 295 ± 3 K in the 390–460 nm region using a non-linear least-squares fit approach

Reference 1	Reference 2	Shift (nm)	Scaling factor	Scale to mean
–	Vandaele et al. [88]	–	1.000	0.983
Vandaele et al. [88]	Merienne et al. [79,80,82,87]	0.00115	0.995	0.988
Vandaele et al. [88]	Harder et al. [84]	0.00118	1.010	0.973
Vandaele et al. [88]	Yoshino et al. [86]	0.00117	0.986	0.997
Vandaele et al. [88]	Vandaele et al. [83]	–0.00012	0.998	0.985
Vandaele et al. [88]	Voigt et al. [89,91,96]	0.00119	0.935	1.051
Vandaele et al. [88]	Vandaele et al. [94,95,97,98]	–0.00051	0.963	1.021

Mean: 0.983 ± 0.026.

### 3.4. Comparison of the NO<sub>2</sub> absorption cross-sections between 230 and 790 nm at temperatures below room temperature (203–280 K)

The following low-temperature NO<sub>2</sub> absorption cross-sections were available in digital form over large spectral intervals:

- Bass et al. (185–410 nm, 235 and 298 K) [67];
- Leroy and coworkers (427–450 nm, 235 and 298 K) [69,70];
- Davidson et al. (264–648 nm, 233, 243, 253, 263, 273, and 298 K) [74];
- Harwood and Jones (313–568 nm, 213, 225, 233, 243, 253, 263, 273, and 298 K) [78];
- Mérienne and coworkers; Coquart and coworkers (200–500 nm, 220, 240, and 293 K) [79,80,82,87];
- Harder et al. (345–550 nm, 217, 230, 238, and 294 K) [84];
- Vandaele et al., 1998 (238–666 nm, 220 and 294 K) [88];
- Burrows et al. (231–794 nm, 221, 241, 273, and 293 K) [90];
- Voigt et al., (250–800 nm, 223, 246, 260, 280, and 293 K) [91,96];
- Bogumil and coworkers (230–1070 nm, 203, 223, 243, 273, and 293 K) [61,92,93];
- Vandaele et al., 2001 (385–724 nm, 220, 240, and 294) [94,95,97,98].

Note that there is only one data set available at 203 K [57,58,61,92,93].

#### 3.4.1. Relative change of the NO<sub>2</sub> absorption cross-sections with temperature

For each set of laboratory cross-sections at different temperatures, we have studied the relative change of the NO<sub>2</sub> absorption cross-sections with temperature. This approach allows the identification of regions where the effect of temperature is dominant, and reduces systematic errors due to the determination of NO<sub>2</sub> amounts during the laboratory measurements.

Note that there has been some controversy about the relative change of the cross-sections with decreasing temperature: in the early studies of Bass et al. and Leroy et al., it was

observed that the absorption cross-sections show an overall decrease of about 10% between room temperature and 235 K. However, all recent studies (i.e. [54,56–58,61,74,78–98]) do not confirm this observation.

In the 300–700 nm region, the relative change of the absorption cross-sections with decreasing temperature is a tilt in the baseline (observed in the data of Davidson et al., Burrows et al., Bogumil et al., but less pronounced in the data of Harwood et al., Harder et al., Vandaele et al., and Voigt et al.) which is accompanied by large changes (up to 60% above 700 nm) in the differential cross-sections. This is due to the change in the thermal population of the lower vibrational and rotational states. The latter observation also indicates the importance of transitions from excited states in the long-wavelength part of the spectrum as already mentioned by Davidson et al. The same authors also interpreted the baseline tilt as an overall shift of the Gaussian part of the NO<sub>2</sub> absorption cross-section spectrum towards longer wavelengths (lower energies) with increasing temperature.

There are large discrepancies concerning the absolute magnitude of the changes of the NO<sub>2</sub> cross-sections with temperature, both concerning the baseline change and the high-resolution (differential) structures. Part of the latter differences might be due to spectral resolution, but there are probably important baseline errors in several data sets.

There is important noise in some data sets towards the edges of the available cross-sections or around regions where the absorption spectra from different measurements have been concatenated. In the room-temperature spectrum by Voigt et al., there are artificial features around 500 nm that show up in the ratios at low temperatures. The data of Burrows et al. seem to contain some residual N<sub>2</sub>O<sub>4</sub> structures at wavelengths below 400 nm at the lowest temperature (221 K).

From the high-resolution spectra of Coquart et al., Harder et al., Vandaele et al., and Voigt et al., it seems that the relative changes of the differential cross-sections with temperature become smaller at wavelengths below 400 nm.

The differential structures change in both directions, and from an inspection of the cross-sections one can see that cross-section maxima become larger and minima become smaller with decreasing temperature. Using room-

temperature cross-sections for low-temperature NO<sub>2</sub> (e.g. in the stratosphere) leads to higher NO<sub>2</sub> columns than really present (see also Roscoe and Hind [77] and Sanders [81]).

### 3.4.2. Comparison of the absolute NO<sub>2</sub> cross-sections at all available wavelengths at temperatures below ambient: 242 ± 4 and 220 ± 3 K

In the following, we have compared the available NO<sub>2</sub> cross-sections at temperatures below ambient: 242 ± 4 and 220 ± 3 K. Because there is less data available at other low temperatures (230–280 K) and only one data set at 203 K [57,58,61,92,93], we have limited the comparisons to these two temperatures.

These comparisons have led to the same observations as already made by inspecting the data at room temperature, namely

- Significant discrepancies due to different spectral resolutions and possible wavelength calibration errors, in particular in the region above 400 nm.
- An overall agreement between the different cross-sections within about 15% in the region between 350 and 500 nm.
- Baseline differences in most of the data at wavelengths below 400 nm (up to 15% above 300 nm and much higher below) and above 500 nm (up to 20% below 600 nm and much higher above).
- Discrepancies in the differential cross-sections leading to an overall offset of the cross-section ratios which do require a non-linear least squares fitting analysis (see below) because of the possible influence of baseline errors.

Although these plots are difficult to interpret since most of the observed differences are due to measurement errors, they indicate that the current accuracy of the laboratory cross-sections of NO<sub>2</sub> at temperatures below 298 K is still limited (the overall agreement between the most recent data sets in the 350–500 nm region is only 10–15%).

### 3.4.3. Comparison of the integrated NO<sub>2</sub> cross-sections at low temperatures

As for the cross-sections at room temperature, we have compared the integrated cross-sections since they are rather insensitive to small wavelength shifts and the ILS.

We could not use the data of Burrows et al. and Bogumil et al. for these comparisons, because these authors already assumed a constant integrated absorption cross-section in the 250–790 nm region (the cross-sections at lower temper-

atures were scaled to the integrated value at room temperature). They derived this hypothesis from the validity of the Born-Oppenheimer approximation (separation of electronic and nuclear wavefunctions). It is clear that this approximation only holds over a certain temperature range (they observed an agreement of the integrated cross-sections of better than 2% from scaling their spectra to the cross-sections of Harwood and Jones in the 400 nm region). A temperature dependence of the integrated cross-section in the 220–295 K range would indicate a significant change of the electronic transition moment as a function of the lower vibrational states.

Note also that Davidson et al. concluded: “*The integral of a plot of  $\sigma$  versus  $1/\lambda$  (264–649 nm) was essentially independent of temperature. . . . The slope of this plot is . . . equal to zero within the uncertainty in the data.*” (their estimated accuracy was ±5%).

Similar conclusions were also drawn by Harwood and Jones: “*It is concluded that any temperature trend in the averaged cross-sections is smaller than the uncertainty in the measurement and therefore a temperature parametrization is meaningless . . . . The variation of cross-section with temperature . . . is solely attributed to experimental scatter. . . . We conclude . . . that the overall spectral shape is independent of temperature.*”

From the comparisons, it seems however possible that there exists a small but systematic increase of the integrated cross-sections with temperature. All data sets agree in this qualitative observation. The increase seems to be smaller when the integration limits extend over the entire absorption system (250–650 nm). The increase is always less than 5%, probably—taking into account the scatter of the data—even <3%. The sudden jump (–6.1% between 238 and 230 K) in the integrated cross-sections of Harder et al. might indicate a systematic error since a change of this magnitude it was not observed by any other author.

Note, that at 240 K, the agreement of the integrated cross-sections available in the 400–500 nm band is better than 4%, and at 220 K better than 5%. Remember that at 295 K, the overall agreement was better than 2.5%.

### 3.4.4. Non-linear least-squares fits of the NO<sub>2</sub> cross-sections between 400–460 nm at 220 ± 3 K

In Table 8, we give the results of non-linear least-squares fits of the NO<sub>2</sub> cross-sections in the 400–460 nm region at 220 ± 3 K. The fits were performed using the same software as used for O<sub>3</sub> and NO<sub>2</sub> (at room temperature).

Table 8

Comparison of NO<sub>2</sub> cross-sections at 220 ± 3 K in the 390–460 nm region using a non-linear least-squares fit approach

Reference 1	Reference 2	Shift (nm)	Scaling factor	Scale to mean
–	Vandaele et al. [88]	–	1.000	0.993
Vandaele et al. [88]	Coquart et al. [80]	–0.00003	0.984	1.023
Vandaele et al. [88]	Harder et al. [84]	–0.00002	1.037	0.971
Vandaele et al. [88]	Voigt et al. [89,91,96]	0.00004	0.782	1.021

Mean: 1.007 ± 0.027. Calculated without using the data of Voigt et al.

Note that the agreement between the different data (after baseline correction and rescaling) concerning the fine structure (residuals) is always better than 5%. The best agreement is obtained between the data of Coquart et al. and Vandaele et al. [88], they agree within 1.6% (rms). The baseline difference between these authors is nearly zero. The cross-sections of Voigt et al. contain a large baseline error (Figs. 16–21) that leads to a 22% change in the scaling factor. The cross-sections by Harder et al. seem to contain more noise than the other data. There is also a negative baseline difference compared to the cross-sections of Coquart et al. and Vandaele et al. [88].

### 3.5. Empirical models for the temperature-dependence of the NO<sub>2</sub> cross-sections in the 240–790 nm region

Generally, three different models have been proposed in the past to reproduce the temperature-dependence of the absorption cross-sections of NO<sub>2</sub>. We have used these three models plus a simplified version of one of them, in order to investigate how well they can reproduce the experimental data.

- The first model [74,85,97,98] uses a linear function:

$$\frac{\sigma(\lambda, T)}{\sigma(\lambda, T_0)} = c_0(\lambda) + c_1(\lambda) \times T$$

where  $T$  is the temperature in K,  $T_0$  is 295 or 273 K, and  $c_0(\lambda)$  and  $c_1(\lambda)$  are wavelength-dependent coefficients. Although there is no real physical interpretation of this model it was concluded by several authors in the past that this function can reproduce the temperature-dependence of the NO<sub>2</sub> cross-sections within the experimental uncertainties.

- The second model [55,90] uses a quadratic polynomial:

$$\frac{\sigma(\lambda, T)}{\sigma(\lambda, T_0)} = c_0(\lambda) + c_1(\lambda) \times T + c_2(\lambda) \times T^2$$

where  $T$  is the temperature in K and  $c_0(\lambda)$ ,  $c_1(\lambda)$ , and  $c_2(\lambda)$  are wavelength-dependent coefficients.

- The third model [54,56,60,89,91,96] uses a double exponential function:

$$\frac{\sigma(\lambda, T)}{\sigma(\lambda, T_0)} = \frac{c_0(\lambda)}{\lambda} \times \exp\left[-\frac{c_1(\lambda)}{T} + c_2(\lambda) \times T\right]$$

where  $T$  is the temperature in K and  $c_0(\lambda)$ ,  $c_1(\lambda)$ , and  $c_2(\lambda)$  are wavelength-dependent coefficients. The latter coefficients are proportional to the temperature-independent transition moment and to the Boltzmann factor of the lower states involved in the transitions.

We have investigated the accuracy of these three models using the experimental data of Bogumil et al. because they cover a large spectral range (13,500–35,000 cm<sup>-1</sup>, i.e. 285–740 nm) and nearly all atmospheric temperatures (203–293 K). The calculations were made in wavenumbers

(cm<sup>-1</sup>), and before the calculations, the experimental data at five temperatures were interpolated to a new grid with a spacing of 5 cm<sup>-1</sup> (0.04–0.3 nm).

One can conclude that all models reproduce the experiments to better than 2% in the 17,500–30,000 cm<sup>-1</sup> region (570–330 nm). There are clearly baseline errors in the experimental data because these differences (up to 2% in the central region around 25,000 cm<sup>-1</sup> and even more on the edges below 17,500 and above 30,000 cm<sup>-1</sup>) are visible in all calculations independently of the model, and they even dominate the differences between the observed and modelled cross-sections (the differences without these baseline errors are about 1% only). Note that even the concatenation point at 400 nm (SCIAMACHY Channel 1 and 2) shows up in the residuals.

Obviously, using an empirical model can partly correct for some of the systematic experimental errors (for example, the differences between modelled and measured cross-sections are of opposite sign for two neighbouring temperatures and show a smooth variation with wavelength—although the cross-sections were fitted point by point—as expected when systematic errors such as baseline drifts or straylight are present). We would therefore recommend to use always an empirical model when NO<sub>2</sub> cross-sections are available at different temperatures (note however that more temperatures than model parameters are required to correct for systematic errors).

The differences between the four models (linear, quadratic, simple and double exponential) are so small that we cannot give any preference to one of these models. The advantage of using a linear model is of course calculation speed which can be important for some applications.

### 3.6. Pressure-dependence of the NO<sub>2</sub> cross-sections in the 240–790 nm region

The first observation of a pressure-dependence of the NO<sub>2</sub> absorption cross-sections in the 240–790 nm region was published by Harder et al. based on high-resolution measurements (0.028 cm<sup>-1</sup> or 0.0006 nm) measured between 441 and 452 nm using a Bruker IFS Fourier-transform spectrometer. They used NO<sub>2</sub>/N<sub>2</sub> mixtures at total pressures between 5 and 600 Torr, and observed changes in the NO<sub>2</sub> cross-sections of up to 40% as a function of total pressure. They concluded that at a spectral resolution of 0.2 nm, the pressure effect between 5 and 600 Torr on the absolute differential cross-section of NO<sub>2</sub> is <0.05%, so that—given the small absorbance of NO<sub>2</sub> even in scattered skylight at high solar zenith angles—this effect is negligible for current remote-sensing applications. They proposed that this pressure effect could be used in the future for NO<sub>2</sub> altitude profile determinations using high-resolution spectra.

Shortly after this publication, another group [88] observed also important effects of total pressure on the absolute absorption cross-sections of NO<sub>2</sub> between 12,000–20,000 cm<sup>-1</sup>. For NO<sub>2</sub> partial pressures varying

only between 0.02 and 1.0 Torr, they observed changes in the cross-sections of up to 40%. It must be emphasized that these large changes were observed at small total pressures and are much higher than expected from infrared measurements (where the pressure broadening coefficient is in the order of  $0.1 \text{ cm}^{-1} \text{ atm}^{-1}$ ). These authors concluded that "... further measurements are required with various buffer gases and  $\text{NO}_2$  mixtures" in order to assess the importance of these effects for atmospheric remote-sensing.

In a third study carried out at the same time [54,60,89,96], new measurements of  $\text{NO}_2$  absorption cross-sections were performed at total pressures of 100 and 1000 mbar (using pure  $\text{N}_2$  as buffer gas) at five different temperatures between 223 and 298 K. These authors also observed an effect of total pressure on the  $\text{NO}_2$  absorption cross-sections, and could reproduce partly the pressure effect by convolution of the low-pressure cross-sections with a Lorentzian profile. Interestingly, they found a linear variation of the pressure-broadening coefficient with temperature (the change is an increase of 30% in the broadening coefficient when going to the lowest temperature) which is in excellent agreement with diode-laser measurements in the mid-infrared and with the current understanding of molecular pressure broadening. However, the magnitude of the pressure broadening coefficient is twice as large as that obtained from measurements in the mid- and near-infrared, probably due to other effects.

A very recent study [97,98] has proposed an empirical model (based on all available measurements) that reproduces the pressure effect within several % at all relevant temperatures.

#### 4. Conclusion

The available laboratory measurements of UV-Vis (240–790 nm) absorption cross-sections of  $\text{O}_3$  and  $\text{NO}_2$  have been critically reviewed taking into account the variation of the cross-sections with temperature (in the 200–300 K range) and with total pressure ( $<1 \text{ atm}$ ). In the most important spectral regions, the agreement between selected data sets is better than 2–3% for both  $\text{O}_3$  [33,34,43,47,48,52,53,55] and  $\text{NO}_2$  [79,80,82–84,88] at all temperatures. Several discrepancies have been identified, mean values were calculated only when appropriate, and empirical models to interpolate the variation of the absorption cross-sections with temperature have been compared.

Future laboratory work is necessary in particular concerning the Huggins bands of ozone at high resolution, but also concerning the relative absorption strengths of the Huggins and Chappuis bands. Recommendations of spectroscopic reference data for atmospheric remote sensing in the UV-Vis and near-infrared are of high importance and should be made available to the community, similar to the recommendations for atmospheric chemistry modelling [99,100], in order to

prepare the database for the new generation of space-borne instruments that will be launched in the next years.

#### Acknowledgements

The author thanks J. Callies, M. Eisinger, A. Hahne, C. Readings, and T. Wehr from the Earth Science Division of ESA-ESTEC for initiating and supporting this work, and K. Bogumil, J. W. Brault, J. Brion, J. P. Burrows, M. Carleer, K. V. Chance, D. Daumont, J.-M. Flaud, A. Goldman, A. Jenouvrier, J. Malicet, M.-F. Mérienne, A. Richter, A.-C. Vandaele, S. Voigt, and K. Yoshino for many helpful discussions.

#### References

- [1] T.E. Graedel, P.J. Crutzen, *Atmospheric Change: An Earth System Perspective*, Freeman, New York, 1993.
- [2] J.H. Seinfeld, S.N. Pandis, *Atmospheric Chemistry and Physics: Air Pollution to Climate*, Wiley, 1997.
- [3] B.J. Finlayson-Pitts, J.N. Pitts, *Chemistry of the Upper and Lower Atmosphere: Theory, Experiments, and Applications*, Academic Press, New York, 1999.
- [4] World Meteorological Organisation, *Scientific Assessment of Ozone Depletion: 1998*, WMO Global Ozone Research and Monitoring Project Report 44, Geneva, 1999.
- [5] R.P. Wayne, *Chemistry of Atmospheres*, 3rd ed., Oxford University Press, Oxford, 2000.
- [6] Intergovernmental Panel on Climate Change, *Climate Change 2001: The Scientific Basis*, Cambridge University Press, Cambridge, 2001.
- [7] J.P. Burrows, M. Weber, M. Buchwitz, V. Rozanov, A. Ladstätter-Weißmayer, A. Richter, R. DeBeek, R. Hoogen, K. Bramstedt, K.-U. Eichmann, M. Eisinger, The global ozone monitoring experiment (GOME): mission concept and first scientific results, *J. Atmos. Sci.* 56 (1999) 151–175.
- [8] J.B. Burrows, E. Hölzle, A.P.H. Goede, H. Visser, W. Fricke, SCIAMACHY—scanning imaging absorption spectrometer for atmospheric cartography, *Acta Astronautica* 35 (1995) 445–451.
- [9] H. Bovensmann, J.P. Burrows, M. Buchwitz, J. Frerick, S. Noël, V.V. Rozanov, SCIAMACHY: mission objectives and measurements modes, *J. Atmos. Sci.* 56 (1999) 127–150.
- [10] J. Orphal, K. Bogumil, A. Dehn, B. Deters, S. Dreher, O.C. Fleischmann, M. Hartmann, S. Himmelmann, T. Homann, H. Kromminga, P. Spietz, A. Türk, A. Vogel, S. Voigt, J.P. Burrows, Laboratory spectroscopy in support of UV-Vis remote-sensing of the atmosphere, in: *Recent Research Developments in Physical Chemistry*, vol. 6, Transworld Research Network, Trivandrum, 2002, pp. 15–34.
- [11] G.L. Humphrey, R.M. Badger, The absorption spectrum of ozone in the visible, *J. Chem. Phys.* 15 (1947) 794–798.
- [12] A. Vassy, E. Vassy, Effect of temperature on the absorption spectrum of ozone: Chappuis bands, *J. Chem. Phys.* 16 (1948) 1163–1164.
- [13] E. Vigroux, Contribution à l'Étude Expérimentale de l'Absorption de l'Ozone, *Ann. Phys.* 8 (1953) 709–762.
- [14] E.C.Y. Inn, Y. Tanaka, Absorption coefficients of ozone in the ultraviolet and visible regions, *J. Opt. Soc. Am.* 43 (1953) 870–873.
- [15] E.C.Y. Inn, Y. Tanaka, Ozone absorption coefficients in the visible and ultraviolet regions, *Adv. Chem. Ser.* 21 (1958) 263–268.
- [16] A.G. Hearn, The absorption of ozone in the ultraviolet and visible regions of the spectrum, *Proc. Phys. Soc.* 78 (1961) 932–940.
- [17] W.B. De More, O. Raper, Hartley band extinction coefficients of ozone in the gas phase and in liquid nitrogen, carbon monoxide, and argon, *J. Phys. Chem.* 68 (1964) 412–414.

- [18] E. Vigroux, Détermination des Coefficients Moyens de l'Absorption de l'Ozone en Vue des Observations Concernant l'Ozone Atmosphérique à l'Aide du Spectromètre Dobson, *Ann. Phys. 2* (1967) 209–215.
- [19] M. Griggs, Absorption coefficients of ozone in the ultraviolet and visible regions, *J. Chem. Phys.* 49 (1968) 857–859.
- [20] E. Vigroux, Coefficients d'absorption de l'ozone dans la bande de Hartley, *Ann. Géophys.* 25 (1969) 169–172.
- [21] J.W. Simons, R.J. Paur, H.A. Webster, E.J. Bair, Ozone ultraviolet photolysis, Part VI, The ultraviolet spectrum, *J. Chem. Phys.* 59 (1973) 1203–1208.
- [22] R.D. Hudson, Absorption cross-sections of stratospheric molecules, *Can. J. Chem.* 52 (1974) 1465–1478.
- [23] W.B. De More, M. Patapoff, Comparison of ozone determination by ultraviolet photometry and gas-phase titration, *Environ. Sci. Technol.* 10 (1976) 897.
- [24] C.M. Penny, Study of temperature dependence of the Chappuis band absorption of ozone, NASA Contract Report 158977, 1979.
- [25] W.D. Komhyr, Dobson spectrophotometer systematic total ozone measurement error, *Geophys. Res. Lett.* 7 (1980) 161–163.
- [26] K.F. Klenk, Absorption coefficients of ozone for the backscatter UV experiment, *Appl. Opt.* 19 (1980) 236–242.
- [27] A.M. Bass, R.J. Paur, UV absorption cross-sections for ozone: the temperature dependence, *J. Photochem.* 17 (1981) 141.
- [28] R.D. McPeters, A.M. Bass, Anomalous atmospheric spectral features between 300 and 310 nm interpreted in light of new ozone absorption coefficient measurements, *Geophys. Res. Lett.* 9 (1982) 227.
- [29] D. Daumont, J. Brion, J. Malicet, Measurement of total atmospheric ozone: consequences entailed by the new value of O<sub>3</sub> absorption cross-sections at 223 K in the 310–350 nm spectral range, *Planet. Space Sci.* 31 (1983) 1229–1234.
- [30] J. Brion, D. Daumont, J. Malicet, New measurements of the absolute absorption cross-sections of ozone at 294 and 223 K in the 310–350 nm spectral range, *J. Phys. (Paris) Lett.* 45 (1984) L57–L60.
- [31] J. Brion, D. Daumont, J. Malicet, P. Marché, Sections Efficaces Absolues de l'Ozone à 298 K aux Longueurs d'Onde de la Lampe au Mercure: Etude Critique des Données Expérimentales Existantes, *J. Phys. (Paris) Lett.* 46 (1985) L105–L110.
- [32] D.E. Freeman, K. Yoshino, J.R. Esmond, W.H. Parkinson, High-resolution absorption cross-section measurements of ozone at 195 K in the wavelength region 240–350 nm, *Planet. Space Sci.* 32 (1984) 239–248.
- [33] A.M. Bass, R.J. Paur, The ultraviolet cross-sections of ozone, Part I, The measurements, in: C.S. Zerefos, A. Ghazi, D. Reidel (Eds.), *Atmospheric Ozone*, Norwell, Mass., 1985, pp. 606–610.
- [34] R.J. Paur, A.M. Bass, The ultraviolet cross-sections of ozone, Part II, Result and temperature dependence, in: C.S. Zerefos, A. Ghazi, D. Reidel (Eds.), *Atmospheric Ozone*, Norwell, Mass., 1985, pp. 611–616.
- [35] K. Mauersberger, D. Hanson, J. Morton, A new ozone standard: the vapor pressure of ozone at liquid argon temperatures, *Geophys. Res. Lett.* 12 (1985) 89–92.
- [36] L.T. Molina, M.J. Molina, Absolute absorption cross-sections of ozone in the 185–350 nm wavelength range, *J. Geophys. Res. D* 91 (1986) 14501–14508.
- [37] K. Mauersberger, D. Hanson, J. Morton, Measurement of the ozone absorption cross-section at the 253.7 nm mercury line, *Geophys. Res. Lett.* 13 (1986) 671–673.
- [38] K. Mauersberger, D. Hanson, J. Barnes, J. Morton, Ozone vapor pressure and absorption cross-section measurements: introduction of an ozone standard, *J. Geophys. Res.* 91 (1987) 8480–8482.
- [39] J. Barnes, K. Mauersberger, Temperature dependence of the ozone absorption cross-section at the 253.7 nm mercury line, *J. Geophys. Res. D* 92 (1987) 14861–14864.
- [40] J.I. Steinfeld, S.M. Adler-Golden, J.W. Gallagher, Critical survey of data on the spectroscopy and kinetics of ozone in the mesosphere and thermosphere, *J. Phys. Chem. Ref. Data* 16 (1987) 911–951.
- [41] J.B. Kerr, I.A. Asbridge, W.F.J. Evans, Intercomparison of total ozone measured by the Brewer and Dobson spectrophotometers in Toronto, *J. Geophys. Res. D* 93 (1988) 11129–11140.
- [42] K. Yoshino, D.E. Freeman, J.R. Esmond, W.H. Parkinson, Absolute absorption cross-section measurements of ozone in the wavelength region 238–335 nm and the temperature dependence, *Planet. Space Sci.* 36 (1989) 395–398.
- [43] J. Malicet, J. Brion, D. Daumont, Temperature dependence of the absorption cross-section of ozone at 254 nm, *Chem. Phys. Lett.* 158 (1989) 293–296.
- [44] M. Cacciani, A. Di Sarra, G. Fiocco, A. Amoroso, Absolute determination of the cross-sections of ozone in the wavelength region 339–355 nm at temperature 220–293 K, *J. Geophys. Res. D* 94 (1989) 8485–8490.
- [45] A. Amoroso, M. Cacciani, A. Di Sarra, G. Fiocco, Absorption cross-sections of ozone in the 590–610 nm region at  $T = 230$  and 299 K, *J. Geophys. Res.* 95 (1990) 20565–20568.
- [46] S.M. Anderson, K. Mauersberger, Laser measurements of ozone absorption cross-sections in the Chappuis band, *Geophys. Res. Lett.* 19 (1992) 933–936.
- [47] D. Daumont, J. Brion, J. Charbonnier, J. Malicet, Ozone UV spectroscopy, Part I, Absorption cross-sections at room temperature, *J. Atmos. Chem.* 15 (1992) 145–155.
- [48] J. Brion, A. Chakir, D. Daumont, J. Malicet, C. Parisse, High-resolution laboratory absorption cross-section of O<sub>3</sub>. Temperature effect, *Chem. Phys. Lett.* 213 (1993) 610–612.
- [49] K. Yoshino, J.R. Esmond, D.E. Freeman, W.H. Parkinson, Measurements of absolute absorption cross-sections of ozone in the 185–254 nm wavelength region, *J. Geophys. Res. D* 98 (1993) 5205–5211.
- [50] W.D. Komhyr, C.L. Mateer, R.D. Hudson, Effective Bass–Paur 1985 ozone absorption coefficients for use with Dobson spectrophotometers, *J. Geophys. Res. D* 98 (1993) 20451–20465.
- [51] J.B. Burkholder, R.K. Talukdar, Temperature dependence of the ozone absorption spectrum over the wavelength range 410–760 nm, *Geophys. Res. Lett.* 21 (1994) 581–584.
- [52] J. Malicet, D. Daumont, J. Charbonnier, C. Chakir, A. Parisse, J. Brion, Ozone UV spectroscopy, Part II, Absorption cross-sections and temperature dependence, *J. Atmos. Chem.* 21 (1995) 263–273.
- [53] J. Brion, A. Chakir, J. Charbonnier, D. Daumont, C. Parisse, J. Malicet, Absorption spectra measurements for the ozone molecule in the 350–830 nm region, *J. Atmos. Chem.* 30 (1998) 291–299.
- [54] S. Voigt, J. Orphal, J.P. Burrows: A Study of Absorption Cross-Sections in the UV and Visible: High-Resolution Absorption Cross-Sections of NO<sub>2</sub> and O<sub>3</sub> at Atmospheric Temperatures, Final Report for the European Space Agency ESA, Prepared by SERCO Europe Ltd., London, 1998.
- [55] J.P. Burrows, A. Richter, A. Dehn, B. Deters, S. Himmelmann, S. Voigt, J. Orphal, Atmospheric remote-sensing reference data from GOME, Part 2, Temperature-dependent absorption cross-sections of O<sub>3</sub> in the 231–794 nm range, *J. Quant. Spectrosc. Rad. Transf.* 61 (1999) 509–517.
- [56] S. Voigt, J. Orphal, J.P. Burrows, UV-Vis absorption cross-sections of NO<sub>2</sub> and O<sub>3</sub> at atmospheric temperatures and pressures by FTS, *Proc. Europ. Sympos. Atm. Meas. Space ESA WPP-161 II* (1999) 471–475.
- [57] K. Bogumil, J. Orphal, S. Voigt, H. Bovensmann, O.C. Fleischmann, M. Hartmann, T. Homann, P. Spietz, J.P. Burrows, Reference spectra of atmospheric trace gases measured with the SCIAMACHY PFM satellite spectrometer, *Proc. Europ. Sympos. Atm. Meas. Space ESA WPP-161 II* (1999) 443–446.
- [58] K. Bogumil, J. Orphal, J.P. Burrows, Temperature-dependent absorption cross-sections of O<sub>3</sub>, NO<sub>2</sub>, and other atmospheric trace gases measured with the SCIAMACHY spectrometer, in: *Proceedings of the ERS-ENVISAT Symposium, ESA-ESTEC*, 2000.
- [59] K. Bogumil, J. Orphal, J.-M. Flaud, J.P. Burrows, Vibrational progressions in the visible and near-ultraviolet absorption spectrum of ozone, *Chem. Phys. Lett.* 349 (2001) 241–248.

- [60] S. Voigt, J. Orphal, K. Bogumil, J.P. Burrows, The temperature dependence (203–293 K) of the absorption cross-sections of O<sub>3</sub> in the 230–850 nm region measured by Fourier-transform spectroscopy, *J. Photochem. Photobiol. A* 143 (2001) 1–9.
- [61] K. Bogumil, J. Orphal, T. Homann, S. Voigt, P. Spietz, O.C. Fleischmann, A. Vogel, M. Hartmann, H. Bovensmann, J. Frerick, J.P. Burrows, Measurements of molecular absorption spectra with the SCIAMACHY pre-flight model: instrument characterization and reference data for atmospheric remote-sensing in the 230–2380 nm region, *J. Photochem. Photobiol. A*, submitted for publication.
- [62] M. Bahou, L. Schriver-Mazzuoli, A. Schriver, Infrared spectroscopy and photochemistry at 266 nm of the ozone dimer trapped in an argon matrix, *J. Chem. Phys.* 114 (2001) 4045–4052.
- [63] Z. Slanina, L. Adamowicz, A computational study of the ozone dimer, *J. Atmos. Chem.* 16 (1993) 41–48.
- [64] J.K. Dixon, The absorption coefficient of nitrogen dioxide in the visible spectrum, *J. Chem. Phys.* 8 (1940) 157–160.
- [65] T.C. Hall Jr., F.E. Blacet, Separation of the absorption spectra of NO<sub>2</sub> and N<sub>2</sub>O<sub>4</sub> in the range of 2400–5000 Å, *J. Chem. Phys.* 20 (1952) 1745–1749.
- [66] H.S. Johnston, R. Graham, Photochemistry of NO<sub>x</sub> and HNO<sub>x</sub> compounds, *Can. J. Chem.* 52 (1974) 1415–1423.
- [67] A.M. Bass, A.E. Ledford Jr., A.H. Laufer, Extinction coefficients of NO<sub>2</sub> and N<sub>2</sub>O<sub>4</sub>, *J. Res. NBS A* 80 (1976) 143–166.
- [68] A.B. Harker, W. Ho, J.J. Ratto, Photodissociation quantum yield of NO<sub>2</sub> in the region 375–420 nm, *Chem. Phys. Lett.* 50 (1977) 394–397.
- [69] E. Hicks, B. Leroy, P. Rigaud, J.-L. Jourdain, and G. Le Bras, Spectres d'Absorption dans le Proche Ultraviolet et Visible des Composés Minoritaires Atmosphériques NO<sub>2</sub> et SO<sub>2</sub> entre 200 et 300 K, *J. Chim. Phys.* 76 (1979) 693–698.
- [70] B. Leroy, P. Rigaud, E. Hicks, Visible absorption cross-sections of NO<sub>2</sub> at 298 and 235 K, *Ann. Geophys. A* 5 (1987) 247–250.
- [71] J.B. Koffend, J.S. Holloway, M.A. Kwok, R.F. Heidner III, High resolution absorption spectroscopy of NO<sub>2</sub>, *J. Quant. Spectrosc. Rad. Transf.* 37 (1987) 449–453.
- [72] J.G. Calvert, S. Madronich, E.P. Gardner, J.A. Davidson, C.A. Cantrell, R.E. Shetter, Mechanism of NO<sub>2</sub> photodissociation in the energy-deficient region at 404.7 nm, *J. Phys. Chem.* 91 (1987) 6339–6341.
- [73] W. Schneider, G.K. Moortgat, G.S. Tyndall, J.P. Burrows, Absorption cross-sections of NO<sub>2</sub> in the UV and visible region (200–700 nm) at 298 K, *J. Photochem. Photobiol. A* 40 (1987) 195–217.
- [74] J.A. Davidson, C.A. Cantrell, A.H. McDaniel, R.E. Shetter, S. Madronich, J.G. Calvert, Visible-ultraviolet absorption cross-sections for NO<sub>2</sub> as a function of temperature, *J. Geophys. Res. D* 93 (1988) 7105–7112.
- [75] T.C. Corcoran, E.J. Beiting, M.O. Mitchell, High-resolution absolute absorption cross-sections of NO<sub>2</sub> at 295, 573, and 673 K at visible wavelengths, *J. Mol. Spectrosc.* 154 (1992) 119–128.
- [76] A. Amoroso, L. Crescentini, G. Fiocco, M. Volpe, New measurements of the NO<sub>2</sub> absorption cross-section in the 440–460 nm region and estimates of the NO<sub>2</sub>–N<sub>2</sub>O<sub>4</sub> equilibrium constant, *J. Geophys. Res. D* 98 (1993) 16857–16863.
- [77] H.K. Roscoe, A.K. Hind, The equilibrium constant of NO<sub>2</sub> with N<sub>2</sub>O<sub>4</sub> and the temperature dependence of the visible spectrum of NO<sub>2</sub>: a critical review and the implications for measurements of NO<sub>2</sub> in the polar stratosphere, *J. Atmos. Chem.* 16 (1993) 257–276.
- [78] M.H. Harwood, R.L. Jones, Temperature dependent ultraviolet-visible absorption cross-sections of NO<sub>2</sub> and N<sub>2</sub>O<sub>4</sub>: low-temperature measurements of the equilibrium constant for 2NO<sub>2</sub>–N<sub>2</sub>O<sub>4</sub>, *J. Geophys. Res. D* 99 (1994) 22955–22964.
- [79] M.F. Mérienne, A. Jenouvrier, B. Coquart, The NO<sub>2</sub> absorption spectrum, Part I, Absorption cross-sections at ambient temperature in the 300–500 nm region, *J. Atmos. Chem.* 20 (1995) 281–297.
- [80] B. Coquart, A. Jenouvrier, M.F. Mérienne, The NO<sub>2</sub> absorption spectrum, Part II, Absorption cross-sections at low temperatures in the 400–500 nm region, *J. Atmos. Chem.* 21 (1995) 251–261.
- [81] R.W. Sanders, Improved analysis of atmospheric absorption spectra by including the temperature dependence of NO<sub>2</sub>, *J. Geophys. Res. D* 101 (1996) 20945–20952.
- [82] A. Jenouvrier, B. Coquart, M.F. Mérienne, The NO<sub>2</sub> absorption spectrum. Part III. The 200–300 nm region at ambient temperature, *J. Atmos. Chem.* 25 (1996) 21–32.
- [83] A.C. Vandaele, C. Hermans, P.C. Simon, M. Van Roozendaal, J.M. Guilmot, M. Carleer, R. Colin, Fourier transform measurement of NO<sub>2</sub> absorption cross-sections in the visible range at room temperature, *J. Atmos. Chem.* 25 (1996) 289–305.
- [84] J.W. Harder, J.W. Brault, P.V. Johnston, G.H. Mount, Temperature dependent NO<sub>2</sub> cross-sections at high spectral resolution, *J. Geophys. Res. D* 102 (1997) 3861–3879.
- [85] B. Kirmse, A. Delon, R. Jost, NO<sub>2</sub> absorption cross-section and its temperature dependence, *J. Geophys. Res. D* 102 (1997) 16089–16098.
- [86] K. Yoshino, J.R. Esmond, W.H. Parkinson, High resolution absorption cross-section measurements of NO<sub>2</sub> in the UV and visible region, *Chem. Phys.* 221 (1997) 169–174.
- [87] M.F. Mérienne, A. Jenouvrier, B. Coquart, J.P. Lux, The NO<sub>2</sub> absorption spectrum. Part IV. The 200–400 nm region at 220 K, *J. Atmos. Chem.* 27 (1997) 219–232.
- [88] A.C. Vandaele, C. Hermans, P.C. Simon, M. Carleer, R. Colin, S. Fally, M.F. Mérienne, A. Jenouvrier, B. Coquart, Measurements of the NO<sub>2</sub> absorption cross-section from 42,000–10,000 cm<sup>-1</sup> (238–1000 nm) at 220 and 294 K, *J. Quant. Spectrosc. Rad. Transf.* 59 (1998) 171–184.
- [89] S. Voigt, J. Orphal, J.P. Burrows: A Study of Absorption Cross-Sections in the UV and Visible: High-Resolution Absorption Cross-Sections of NO<sub>2</sub> and O<sub>3</sub> at Atmospheric Temperatures, Final Report for the European Space Agency ESA, Prepared by SERCO Europe Ltd., London, 1998.
- [90] J.P. Burrows, A. Dehn, B. Deters, S. Himmelmann, A. Richter, S. Voigt, J. Orphal, Atmospheric remote-sensing reference data from GOME. Part 1. Temperature-dependent absorption cross-sections of NO<sub>2</sub> in the 231–794 nm range, *J. Quant. Spectrosc. Rad. Transf.* 60 (1998) 1025–1031.
- [91] S. Voigt, J. Orphal, J.P. Burrows, UV-Vis absorption cross-sections of NO<sub>2</sub> and O<sub>3</sub> at atmospheric temperatures and pressures by FTS, *Proc. Europ. Sympos. Atm. Meas. Space ESA WPP-161 2* (1999) 471–475.
- [92] K. Bogumil, J. Orphal, S. Voigt, H. Bovensmann, O.C. Fleischmann, M. Hartmann, T. Homann, P. Spietz, J.P. Burrows, Reference spectra of atmospheric trace gases measured with the SCIAMACHY PFM satellite spectrometer, *Proc. Europ. Sympos. Atm. Meas. Space ESA WPP-161 II* (1999) 443–446.
- [93] K. Bogumil, J. Orphal, J.P. Burrows: Temperature-dependent absorption cross-sections of O<sub>3</sub>, NO<sub>2</sub>, and other atmospheric trace gases measured with the SCIAMACHY spectrometer, in: *Proceedings of the ERS-ENVISAT Symposium, ESA-ESTEC, 2000.*
- [94] A.C. Vandaele, C. Hermans, S. Fally, M. Carleer, R. Colin, M.F. Mérienne, A. Jenouvrier, High-resolution measurement of the NO<sub>2</sub> visible absorption cross-section, in: *Proceedings of the EGS Symposium on Temperature and Pressure Effects, Nice, France, 2000.*
- [95] A.C. Vandaele, C. Hermans, C. Fayt, S. Fally, M. Carleer, R. Colin, M.F. Mérienne, A. Jenouvrier, B. Coquart, High-Resolution Fourier Transform Measurement of the NO<sub>2</sub> Visible Absorption Cross-Section: Temperature and Pressure Influences on Its Atmospheric Detection, *JRS Symposium, St. Petersburg (Russia), 2000.*
- [96] S. Voigt, J. Orphal, J.P. Burrows, The Temperature- and Pressure-Dependence of the Absorption Cross-sections of NO<sub>2</sub> in the

- 250–800 nm Region Measured by Fourier-Transform Spectroscopy, *J. Photochem. Photobiol. A* 149 (2002) 1–7.
- [97] A.C. Vandaele, C. Hermans, S. Fally, M. Carleer, R. Colin, M.F. Mérienne, A. Jenouvrier, and B. Coquart, High-Resolution Fourier Transform Measurement of the NO<sub>2</sub> Visible and Near-Infrared Absorption Cross-Section: Temperature and Pressure Effects, *J. Geophys. Res. D* 107 (2002) D 18, 4348, doi: 10.129/2001JD000971.
- [98] C. Vandaele, C. Hermans, S. Fally, M. Carleer, M.F. Mérienne, A. Jenouvrier, R. Colin, Absorption cross-section of NO<sub>2</sub>: simulation of temperature and pressure effects, *J. Quant. Spectrosc. Rad. Transf.* 76 (2003) 373–391.
- [99] W. B. DeMore, S. P. Sander, D. M. Golden, R. F. Hampson, M. J. Kurylo, C. J. Howard, R. A. Ravishankara, C. E. Kolb, and M. J. Molina, Chemical Kinetics and Photochemical Data for Use in Stratospheric Modelling, Evaluation No. 12, JPL Publication No. 97-4, 1997.
- [100] IUPAC Subcommittee on Gas Kinetic Data Evaluation, Evaluated Kinetic and Photochemical Data, <http://www.iupac-kinetic.ch.cam.ac.uk>, updated December 2001.